Inorganic Chemistry

Article

pubs.acs.org/IC

# Nonoxido Vanadium(IV) Compounds Involving Dithiocarbazate-Based Tridentate ONS Ligands: Synthesis, Electronic and Molecular Structure, Spectroscopic and Redox Properties

Sanchita Kundu,[†] Dhrubajyoti Mondal,[†] Kisholoy Bhattacharya,[†] Akira Endo,[‡] Daniele Sanna,[#] Eugenio Garribba,*[,§] and Muktimoy Chaudhury*[,†]

[†]Department of Inorganic Chemistry, Indian Association for the Cultivation of Science, Kolkata 700032, India

[‡]Department of Materials and Life Sciences, Faculty of Science and Technology, Sophia University, 7-1 Kioi-cho, Chiyoda-ku, Tokyo 102-8554, Japan

[#]Istituto CNR di Chimica Biomolecolare, Trav. La Crucca 3, I-07040 Sassari, Italy

[§]Dipartimento di Chimica e Farmacia and Centro Interdisciplinare per lo Sviluppo della Ricerca Biotecnologica e per lo Studio della Biodiversità della Sardegna, Università di Sassari, Via Vienna 2, I-07100 Sassari, Italy

Supporting Information

**ABSTRACT:** A new series of nonoxido vanadium(IV) compounds $[VL_2]$ (L = $L^1$–$L^3$) (**1**–**3**) have been synthesized using dithiocarbazate-based tridentate Schiff-base ligands $H_2L^1$–$H_2L^3$, containing an appended phenol ring with a *tert*-butyl substitution at the 2-position. The compounds are characterized by X-ray diffraction analysis (**1**, **3**), IR, UV-vis, EPR spectroscopy, and electrochemical methods. These are nonoxido $V^{IV}$ complexes that reveal a rare distorted trigonal prismatic arrangement around the "bare" vanadium centers. Concerning the ligand isomerism, the structure of **1** and **3** can be described as intermediate between *mer* and *sym-fac* isomers. DFT methods were used to predict the geometry, **g** and $^{51}$V **A** tensors, electronic structure, and electronic absorption spectrum of compounds **1**–**3**. Hyperfine coupling constants measured in the EPR spectra can be reproduced satisfactorily at the level of theory PBE0/VTZ, whereas the wavelength and intensity of the absorptions in the UV-vis spectra at the level CAM-B3LYP/gen, where "gen" is a general basis set obtained using 6-31+g(d) for S and 6-31g for all the other elements. The results suggest that the electronic structure of **1**–**3** can be described in terms of a mixing among V-$d_{xy}$, V-$d_{xz}$, and V-$d_{yz}$ orbitals in the singly occupied molecular orbital (SOMO), which causes a significant lowering of the absolute value of the $^{51}$V hyperfine coupling constant along the *x*-axis. The cyclic voltammograms of these compounds in dichloroethane solution display three one-electron processes, two in the cathodic and one in the anodic potential range. Process A ($E_{1/2}$ = +1.06 V) is due to the quasi-reversible V(IV/V) oxidation while process B at $E_{1/2}$ = −0.085 V is due to the quasi-reversible V(IV/III) reduction, and the third one (process C) at a more negative potential $E_{1/2}$ = −1.66 V is due to a ligand centered reduction, all potentials being measured vs Ag/AgCl reference.

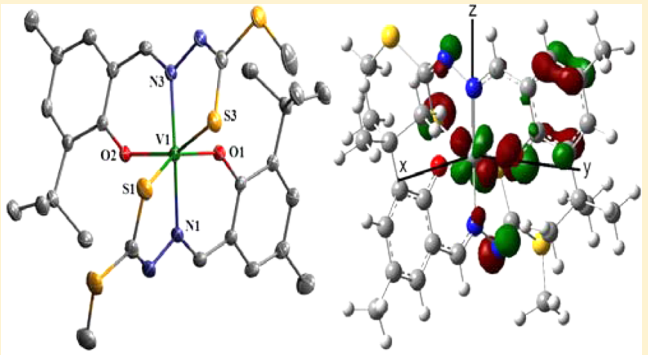


## INTRODUCTION

Vanadium is an important trace element for different organisms.[1] It is present in at least two enzymes, such as vanadium-dependent haloperoxidases[2] and nitrogenases,[3] and it is accumulated in concentrations up to 0.3 M in the vanadocytes of ascidians and polychaete worms.[4] Vanadium also has an important role in the human organism, and it is probably involved in the regulation of phosphate metabolism.[5] Over the last years, it has been demonstrated that many vanadium compounds have therapeutic effects,[6−8] whose structure−activity[9] and reactivity−activity relationship,[10] and biotransformation in the blood has been recently investigated.[11,12]

The most stable V oxidation states in nature are +3, +4, and +5.[1,5] In its higher oxidation states (+4 and +5), vanadium is oxophilic and forms a large varieties of oxido species both in solution as well as in the solid state involving terminal and bridging V−O bonds.[1] Between these types, the multiply bonded V═O terminal bond is extremely inert ($T_{1/2}$ for O-exchange with bulk water is ca. 400 min) with unusually high V═O bond energy (atomization energy, 140 kcal/mol). This is primarily because of the strong p$\pi$ → d$\pi$ donation from the terminal oxido group to the vanadium center.

**Received:** February 13, 2015
**Published:** June 10, 2015





DOI: 10.1021/acs.inorgchem.5b00359
*Inorg. Chem.* 2015, 54, 6203−6215

**Scheme 1. Schematic Presentation for the Formation of Compounds 1−3**

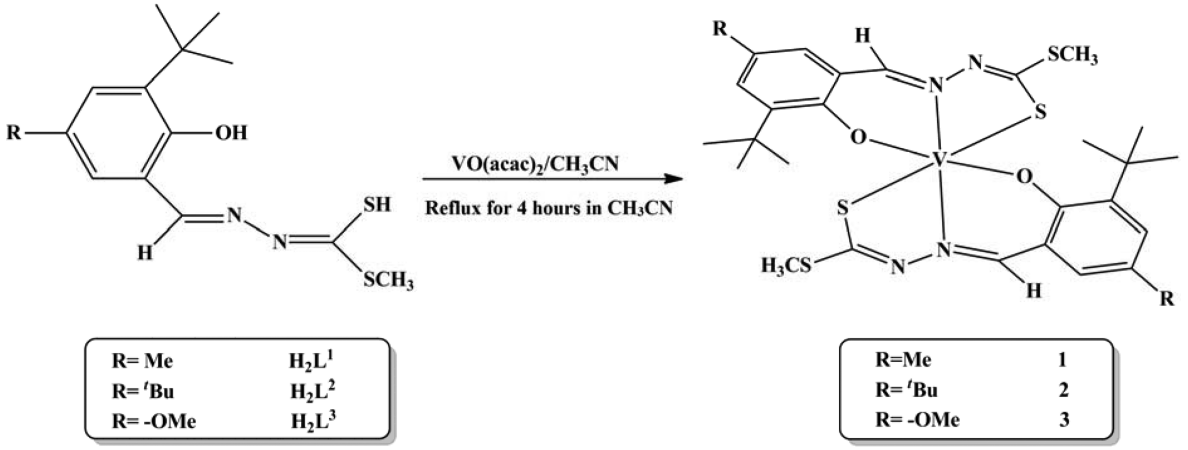


The formation of nonoxido or "bare" vanadium(IV) complexes is a somewhat uncommon, because the strong V═O bond must be broken and the oxido ligand may have to leave the complex, probably as a water molecule. However, rather interestingly in biological domain, two V species free of oxido group exist.[13,14] One of these is a blue compound (named amavadin), isolated from a particular variety of *Amanita* mushroom,[1,13] which is structurally verified to be an eight-coordinated nonoxido vanadium(IV) complex.[15] The second form of nonoxido vanadium is found in the co-factor of an alternative form of nitrogenase, called VNase, which catalyzes the biological conversion of atmospheric dinitrogen to bioavailable ammonia.[5,14] It is a V−Fe cluster compound containing a "bare" $V^V$ center, which is believed to have an analogous structure to FeMoco co-factor of nitrogenase.[16]

All these information have inspired the coordination chemists to synthesize and investigate nonoxido $V^{IV}$ and $V^V$ complexes over the last 30 years. Unfortunately until to date, such compounds are limited in number, because of the extreme inertness of the V═O terminal bonds that stood as an impediment to their facile synthesis. A search within the Cambridge Structural Database[17] shows that the number of nonoxido V species still remains relatively scarce, and almost all of these compounds have vanadium centers in six coordination.[18−25] The formation of these "bare" species is significantly favored by the preorganization of the tridentate ligand, as in the case of *cis*-inositol derivatives.[26] Recently, four- and five-coordination nonoxido $V^{IV}$ species with $VO_4$[27] and $VNO_4$[28] coordination have been reported. In the six-coordinated species, the ligand determines the geometry (octahedral or trigonal prismatic),[24a] the ground state ($d_{xy}$ or $d_{z^2}$),[29] the isomerism (facial or meridional when the ligand is tridentate),[24h,25] and the spectroscopic behavior (EPR and UV-vis responses).[18e,30] However, the electronic structure of these species and their relationship with EPR and electronic absorption spectral properties is still remaining unclear.

We recently reported the synthesis, structures, spectroscopic properties, and redox chemistry of many oxido vanadium compounds using a variety of phenol-based dithiocarbazato Schiff-base ligands.[31] The vanadium centers in these compounds are various types of oxido species. Herein, we report a new family of nonoxido vanadium(IV) compounds (**1**−**3**) through a single-pot synthesis using similar type of dithiocarbazate-based ligands ($H_2L^1$−$H_2L^3$) involving the mandatory presence of *tert*-butyl group as substituent at 2-position of the phenol ring (the ligands are shown in Scheme 1). The compounds have been characterized by single-crystal X-ray diffraction analysis that confirms a rare trigonal prismatic structure for these compounds. Their unusual spectroscopic properties (both UV-vis and EPR) have been interpreted for the first time by simulation studies involving rigorous DFT calculations.

## EXPERIMENTAL AND COMPUTATIONAL SECTION

**Materials.** The solvents were reagent-grade, dried by standard procedure[32] and distilled under nitrogen prior to their use. The ligands $H_2L^1$−$H_2L^3$ were prepared according to literature procedure.[33] $[V^{IV}O(acac)_2]$ was synthesized by a reported method.[34] All other reagents were commercially available and used as-received.

**Synthesis of the Complexes.** *$[V^{IV}(L^1)_2]$ (**1**).* To a stirred solution of $[V^{IV}O(acac)_2]$ (0.066 g, 0.25 mmol) in acetonitrile (30 mL) was added the solid ligand $H_2L^1$ (0.15 g, 0.5 mmol) and the solution was allowed to reflux for 4 h. The resulting dark solution was then cooled to room temperature and filtered. The filtrate volume was reduced to ca. 15 mL by rotary evaporation and kept in the air for slow evaporation when dark green crystals of compound **1** were obtained after ∼2 days. These were collected by filtration, washed with acetonitrile and dried over $CaCl_2$. Yield: 0.083 g (52%). Anal. Calcd for $C_{28}H_{36}N_4O_2S_4V$: C, 52.56%; H, 5.67%; N, 8.76%. Found: C, 52.47%; H, 5.53%; N, 8.73%. FT-IR bands (KBr pellet, $cm^{-1}$) 1575 m, 1543 vs, 1332 s, 1294 s, 1263 m, 1205 m, 1022 s, 973 s, 844 s, 775 m, 557 s. ESI-MS (positive) in $CH_2Cl_2$: *m*/*z* 640.13 $[M+H]^+$, 662.10 $[M+Na]^+$.

*$[V^{IV}(L^2)_2]$ (**2**).* This compound was prepared following an identical method as described for compound **1**, using the ligand $H_2L^2$ instead of $H_2L^1$. Yield: 0.103 g (57%). Anal. Calcd for $C_{34}H_{48}N_4O_2S_4V$: C, 56.41%; H, 6.68%; N, 7.74%. Found: C, 56.63%; H, 6.52%; N, 7.78%. FT-IR bands (KBr pellet, $cm^{-1}$) 1577 s, 1539 vs, 1473 m, 1361 m, 1299 m, 1271 m, 1249 s, 1020 s, 977 s, 848 s, 775 w, 551 s. ESI-MS (positive) in $CH_2Cl_2$: *m*/*z* 724.22 $[M+H]^+$.

*$[V^{IV}(L^3)_2]$ (**3**).* This compound was prepared following an identical method as described for compound **1**, using the ligand $H_2L^3$ instead of $H_2L^1$. Yield: 0.090 g (54%). Anal. Calcd for $C_{28}H_{36}N_4O_4S_4V$: C, 50.06%; H, 5.40%; N, 8.34%. Found: C, 49.31%; H, 5.21%; N, 8.22%. FT-IR bands (KBr pellet, $cm^{-1}$) 1604 m, 1585 m, 1549 s, 1417 w, 1382 w, 1338 m, 1288 m, 1211 m, 1161 m,1058 s, 985 s, 777 vs, 702 w, 605 w, 567 w, 493 w. ESI-MS (positive) in $CH_2Cl_2$: *m*/*z* 672.11 $[M+H]^+$.

**Physical Measurements.** Elemental analyses (for C, H, and N) were performed at IACS on a Perkin−Elmer Model 2400 Series II CHN Analyzer. IR spectroscopic measurements were made on samples prepared as KBr pellets using a Shimadzu Model 8400S FT-IR spectrometer. For UV-visible spectra in solution, a Perkin−Elmer Model Lambda 950 UV/vis/NIR spectrophotometer was


DOI: 10.1021/acs.inorgchem.5b00359
*Inorg. Chem.* 2015, 54, 6203−6215

employed. The electrospray ionization mass spectra (ESI-MS) (in positive ion mode) were measured on a Micromass QTOF YA 263 Mass Spectrometer. EPR spectra were recorded in toluene on a JEOL Model JES-FA 300 X-band spectrometer, equipped with a standard low-temperature (77 K) apparatus and data processing system (ESPRIT 330). Cyclic voltammograms (CVs) of the compounds were recorded in dichloroethane or dichloromethane solution using a BAS model 100 B/W electrochemical workstation coupled with a glassy carbon working and a platinum wire counterelectrode. Ag/AgCl was used for reference and $Fc/Fc^+$ couple as the internal standard.[35] Solutions were ~1.0 mM in samples and contained 0.1 M TBAP as supporting electrolyte. Bulk electrolyses were carried using a platinum-gauze working electrode at 298 K.

**X-ray Crystallography.** Diffraction quality crystals of compound **1** (block, dark green, 0.23 mm × 0.19 mm × 0.11 mm) and compound **3** (block, dark green, 0.18 mm × 0.16 mm × 0.12 mm) were collected from their respective reaction pots containing acetonitrile solvent. Unfortunately, diffraction-quality crystals of compound **2** could not be grown, despite of our repeated attempts. The crystals were mounted on glass fiber without any protection. Intensity data for the compounds were measured at 298 K, employing a Bruker SMART APEX II CCD diffractometer equipped with a monochromatized Mo K$\alpha$ radiation ($\lambda$ = 0.71073 Å) source. No crystal decay was observed during the data collections. The intensity data were corrected for empirical absorption. In all cases, absorption corrections based on multiscans using the SADABS software[36] were applied. The structures were solved by direct methods[37] and refined on $F^2$ by a full-matrix least-squares procedure,[38] based on all data minimizing $R = \sum||F_0| - |F_c||/\sum|F_0|$, $wR = [\sum[w(F_0^2 - F_c^2)^2]/\sum(F_0^2)^2]^{1/2}$, and $S = [\sum[w(F_0^2 - F_c^2)^2]/(n-p)]^{1/2}$. SHELXL-97 was used for both structure solutions and refinements.[38] All non-hydrogen atoms were refined anisotropically. The hydrogen atom positions were calculated and isotropically fixed in the final refinements [$d$(C−H) = 0.95 Å, with the isotropic thermal parameter of $U_{iso}$(H) = 1.2$U_{iso}$(C)]. The SMART and SAINT-plus software packages[39] were used for data collection and reduction, respectively. Crystallographic diagrams were drawn using the DIAMOND software package.[40]

**DFT Calculations.** The geometries of compounds **1**−**3** were optimized in the gas phase with Gaussian 09 (revision C.01) software,[41] using the hybrid exchange-correlation functional B3P86,[42,43] and a general basis set obtained using 6-311+g(d)[44] for S and 6-311g[44] for all other atoms. The functional B3P86 ensures a good degree of accuracy in the prediction of the structures of first-row transition-metal complexes,[45] and particularly of vanadium compounds.[46]

The **g** and $^{51}$V **A** tensor were calculated using the functional PBE0[47] and VTZ basis set with ORCA software,[48] according to the procedures published in the literature.[49] It must be taken into account that, for a $V^{IV}$ species, the $A_z$ value is usually negative, but its absolute value is usually reported in the literature. The theory background was described in detail elsewhere.[50,51]

Time-dependent density functional theory (TD-DFT) calculations[52] were used to predict the excited states of **1** and obtain the expected electronic absorption spectrum. The calculations were carried out using a general basis set (6-31g set for V, O, C, H, and N and 6-31+g(d) for S) and changing the functional on the geometry simulated in the gas phase. The following functional were used: VSXC,[53] HCTH,[54] BP86,[43,55] B1LYP,[56,57] B3LYP,[42,58] PBE0,[47] mPW1PW91,[59] HSEH1PBE,[60] BHandHLYP,[41] APFD,[61] WB97XD,[62] and CAM-B3LYP.[63] The electronic absorption spectrum of **1** was generated using Gauss View version 4.1 software.[64]

## RESULTS AND DISCUSSION

**Syntheses.** Nonoxido vanadium(IV) compounds $[V^{IV}(L)_2]$ (L = $L^1$−$L^3$, compounds **1**−**3**) are obtained in moderate yields (ca. 50%) when stoichiometric amounts of the tridentate dithiocarbazate-based Schiff-base ligands ($H_2L^1$−$H_2L^3$) and the vanadium(IV) precursor compound $[V^{IV}O(acac)_2]$ are refluxed for ~4 h in acetonitrile under aerobic environment (Scheme 1). In some of our earlier communications, it has been reported that the reactions of $[V^{IV}O(acac)_2]$ with similar types of tridentate ONS donor ligands ($H_2L$) have produced solvated compounds $[V^{IV}OL(solvent)]$ as putative intermediates which ultimately get transformed into the products of the type $[LOV^{IV}B]$[31a] in the presence of various nitrogenous bases (B) or into anionic *cis*-dioxido $[V^VO_2L]^-$ products when allowed to interact with various cationic substrates.[31c,f] Thus, in all the previous reports, the products were oxido-vanadium compounds in the oxidation states +4 and +5. However, in the present case, we get the nonoxido vanadium(IV) compounds as the exclusive product with the ligands $H_2L^1$−$H_2L^3$, all of which show mandatory presence of *tert*-butyl group as substituent in 2-position of the phenol ring in the ligand framework (Scheme 1). Presence of this substituent probably increases the donor strength of the phenolate oxygen, resulting in strong $\sigma$ and $\pi$ donation to the vanadium(IV) center and thus compensates for the strong $\pi$-electron donation from the terminal oxido ligand and helps in removing the oxido group as water to generate the "bare" $V^{IV}$ products. Similar influence of ligands with associated *tert*-butyl group in the formation of nonoxido vanadium compounds has been reported earlier.[25]

IR spectra of compounds **1**−**3** have been summarized in the Experimental and Computational Section. The spectra show all the characteristic bands of the participating dithiocarbazate ligands, which include a strong signature band at ~1577−1583 $cm^{-1}$ due to $\nu$(C=N) vibration,[31e] together with a strong band in the region near ~1539−1550 $cm^{-1}$, because of $\nu$(C−O/phenolate) stretching.[31e] The loss of oxido ligand in the products is confirmed by the complete absence of the strong characteristic $\nu$(V=O) stretch in the 900−1000 $cm^{-1}$ region,[65] thus indicating the "bare" vanadium status in these compounds.

**Mass Spectrometry.** ESI-mass spectrometric data (in the positive ion mode), measured in dichloromethane, for complexes **1**−**3** have been listed in the Experimental and Computational Section. Compounds **1**−**3** show molecular ion peaks due to the $[M+H]^+$ species. Compound **1** also shows an additional peak due to an $[M+Na]^+$-type ionic entity. The observed isotopic distributions and their simulation patterns are in agreement with these assigned formulations, as shown in Figure 1 for the representative compound **1**.

**Description of Crystal Structures.** Crystal and molecular structures of compounds **1** and **3** have been determined. A summary of their relevant crystallographic data and the final refinement details are given in Table 1. Figures 2 and 3 display the molecular structures and atom labeling schemes for **1** and **3**,

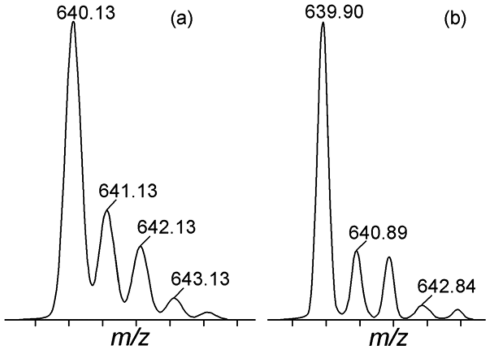


**Figure 1.** Molecular ion peak in the ESI mass spectrum (positive) for complex **1**, measured in dichloromethane, with (a) simulated and (b) observed isotope distribution.



DOI: 10.1021/acs.inorgchem.5b00359
*Inorg. Chem.* 2015, 54, 6203−6215

**Table 1. Summary of X-ray Crystallographic Data for Complexes 1 and 3**

| parameter | 1 | 3 |
|---|---|---|
| composition | $C_{28}H_{36}N_4O_2S_4V$ | $C_{28}H_{36}N_4O_4S_4V$ |
| formula wt | 639.79 | 671.79 |
| crystal system | triclinic | monoclinic |
| space group | $P\bar{1}$ | $P2_1/n$ |
| $a$ (Å) | 10.0076(17) | 12.1166(11) |
| $b$ (Å) | 13.069(2) | 18.6745(16) |
| $c$ (Å) | 13.828(2) | 13.8081(13) |
| $\alpha$ (deg) | 66.593(3) | 90 |
| $\beta$ (deg) | 81.005(3) | 92.784(5) |
| $\gamma$ (deg) | 69.513(3) | 90 |
| $V$ (Å$^3$) | 1554.4(5) | 3120.7(5) |
| $\rho_{calc}$ (g cm$^{-3}$) | 1.367 | 1.430 |
| temp (K) | 298(2) | 298(2) |
| $\lambda$, Mo K$\alpha$ (Å) | 0.71073 | 0.71073 |
| Z | 2 | 4 |
| $F(000)$ ($\mu$ mm$^{-1}$) | 670/0.620 | 1404/0.626 |
| $2\theta_{max}$ (deg) | 52.00 | 55.15 |
| reflections collected/unique | 15912/6096 | 44244/7039 |
| $R_{int}$/GOF on $F^2$ | 0.0274/1.093 | 0.0761/1.105 |
| No. of parameters | 364 | 380 |
| $R1(F_0)$, $wR2(F_0)$ (all data) | 0.0381, 0.1283 | 0.0557, 0.1481 |
| largest diff. peak, deepest hole (eÅ$^{-3}$) | 0.267, −0.670 | 0.973, −0.526 |

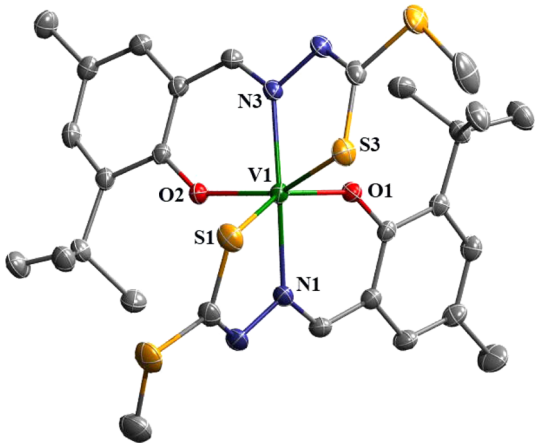


**Figure 2.** Molecular structure and atom labeling scheme for compound **1** with thermal ellipsoids drawn at the 30% probability level. Hydrogen atoms have been omitted for clarity.

respectively. These structures provide confirmatory evidence in support of the presence of nonoxido vanadium center in these complexes. Their selected metrical parameters are summarized in Table S1 in the Supporting Information. The compounds have grossly similar structures and a generic description of these will be provided, considering **1** as a representative example. Identical atom-labeling schemes have been adopted for both the structures for easy comparison of their relevant metrical parameters. Compound **1** crystallizes in triclinic space group $P\bar{1}$ with two molecular mass units accommodated per unit cell, whereas compound **3** crystallizes in the monoclinic space group $P2_1/n$ with four molecular mass units accommodated per cell.

The vanadium(IV) center in this mononuclear complex is six-coordinated, completed by a pair of doubly deprotonated tridentate ONS donor ligands, providing a highly distorted

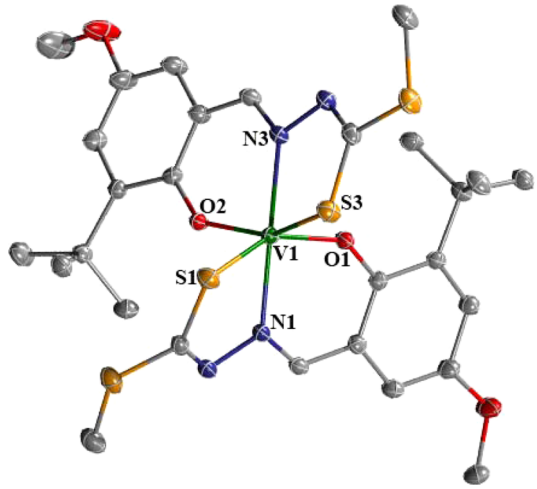


**Figure 3.** Molecular structure and atom labeling scheme for compound **3** with thermal ellipsoids drawn at the 30% probability level. Hydrogen atoms have been omitted for clarity.

geometry as revealed from a skeletal view of the compound (Figure 4). The *trans* angles N3−V1−N1, 162.14(6)° [162.37(9)° for **3**]; O1−V1−S1, 147.75(4)° [147.88(7)°]; and O2−V1−S3, 148.21(5)° [149.29(7)°] have shown substantial deviation from linearity, approaching more toward a trigonal prismatic arrangement (expected angle = 135°) of distorted nature as reported in the literature with related tridentate biprotic ligands.[24a,e,l] Each tridentate ligand in this complex forms a five- and a six-membered chelate ring. The dihedral angles between these ring planes are 18.77° and 16.23° (21.31° and 15.00° for **3**), thus providing folded ligand structures that contribute to the overall trigonal prismatic geometry. As shown in Figure 4, the donor atoms O(1), S(3), and N(3) form one triangular face of the trigonal prism while N(1), S(1), and O(2) form the other triangular face. The dihedral angle between these two triangular faces is 9.38° in compound **1** and 9.52° in **3**. Both these tridentate ligands ($H_2L$) are fully deprotonated, each contributing with two negative charges to generate neutral [$V^{IV}L_2$]-type complexes. The V−O, V−N, and V−S distances are in the normal range as reported in the literature.[24,25]

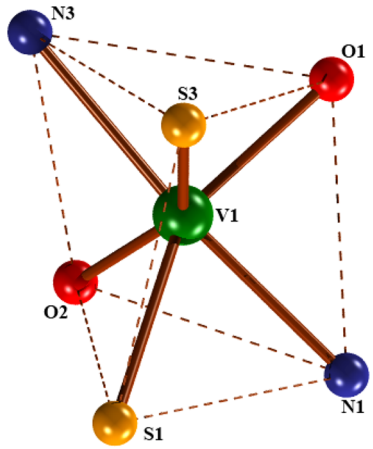


**Figure 4.** Skeletal view of the trigonal prismatic structure in compounds **1** and **3**.


DOI: 10.1021/acs.inorgchem.5b00359
*Inorg. Chem.* 2015, 54, 6203−6215

A hexa-coordinated structure formed by a tridentate ligand can be described in terms of three isomeric forms, viz. meridional (*mer*), symmetric facial (*sym-fac*) and unsymmetric facial (*unsym-fac*). These three possibilities are depicted in Scheme 2 for an ONS donor ligand such as $L^1$ (**1**), $L^2$ (**2**), and $L^3$ (**3**). A high planarity of the ligand favors the meridional coordination, as with $V^{IV}$ complexes of 3,5-bis(2-hydroxyphenyl)-1-phenyl-1*H*-1,2,4-triazole ($H_2hyph^{Ph}$) and 2,6-bis(2-hydroxyphenyl)pyridine ($H_2bhpp$).[24j,66,67] For tridentate ligands with a flexible backbone, the facial as well as the meridional coordination modes are possible; for example, with iminodiacetic acid, the facial coordination is preferred,[68] whereas the reverse behavior has been reported for methylamino-*N*,*N*-bis(2-methylene-4,6-dimethylphenol).[69] With 2,2′-dihydroxyazobenzene (Hdhab) and α-(2-hydroxy-5-methylphenylimino)-*o*-cresol (Hmpic) ligands, the nonoxido $V^{IV}$ compounds have distorted unsymmetric facial isomeric form.[24k]

**Scheme 2. Possible Isomers for Hexacoordinated Nonoxido $V^{IV}$ Structures Formed by a Tridentate ONS Ligand: (a) *mer*, (b) *sym-fac*, and (c) *unsym-fac***

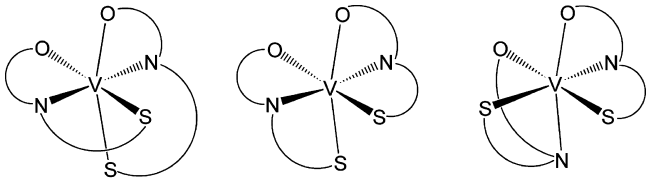


The structures of complexes **1** and **3** can be described by several geometrical parameters: (i) the twist angle Φ, which measures the angle between the two triangular faces of side *s* describing the coordination polyhedron (60° for an octahedron with the two triangles staggered and 0° for a trigonal prism with the two triangles eclipsed);[18d] (ii) the angle Θ, formed by the donors in *trans* to the vanadium (180° for an octahedron and 135° for trigonal prism); (iii) the angle Ω, formed by the two external donors of each ligand with vanadium (180° for *mer* and 90° for *fac* isomers); (iv) the angle Ψ, formed by the two external donors of each ligand molecule with the central donor; (v) the ratio *s*/*h* and *s*/*a*, where *h* is the distance between the two triangles and *a* is the mean metal−ligand bond length (they are 1.225 and 1.414 for an octahedron, and 1.000 and 1.309 for a trigonal prism). The values for the angles Φ and Θ, as revealed from the X-ray crystal structures of **1** and **3**, are in the range 26.8°−27.2° and 152.7°−153.2°, while those of the parameters *s*/*h* and *s*/*a* are 1.361 and 1.100; all these values are intermediate between those expected for a regular octahedron and a trigonal prism (see also Table 2). Concerning the ligand isomerism, the structures of **1** and **3** can be described as intermediate between *mer* and *sym-fac*. In particular, the angle Ω, which should be 180° for the *mer* isomer and 90° for the *fac* isomer, is 148.0° for **1** and 148.6° for **3** (mean values).

**Optimization of the $V^{IV}$ Structures and Comparison with the Experimental X-ray Structures.** The geometry of compounds **1**−**3** was optimized with Gaussian 09 software through DFT methods. The optimized structures are shown in Figure 5. It can be noticed that the prediction of the structural details (bond lengths and angles) is very good; in particular, the V−donor (donor = O, N, S) distances are very close to the experimental values. The optimization of the structure of compound **2** suggests that it should be very similar to **1** and **3**. The experimental and calculated parameters are summarized in Table 2.

It can be noticed that the distortion of a potential meridional toward a facial structure (probably induced by the long V−S length) results in a significant distortion of the octahedral geometry toward the trigonal prism with experimental Φ values of 26.8° and 27.2° (calculated in the range 30.9°−32.1°). Also, the angle Ω is indicative of the arrangement of the ligands, with respect to the metal ion, and assumes the values of 148.0°−148.6° (experimental) and 150.2°−151.1° (calculated).

**EPR Spectroscopy and Prediction of the $^{51}V$ Hyperfine Coupling Constants.** EPR spectroscopy is the tool used

**Table 2. Experimental and Calculated Geometrical Parameters for Complexes 1−3[a]**

| | 1 | | 2 | 3 | |
|---|---|---|---|---|---|
| complex | experimental | calculated | calculated | experimental | calculated |
| bond length, Å | | | | | |
| V−O | 1.858, 1.865 | 1.858, 1.863 | 1.860, 1.963 | 1.858, 1.861 | 1.855, 1.864 |
| V−N | 2.104, 2.099 | 2.104, 2.104 | 2.104, 2.106 | 2.098, 2.118 | 2.101, 2.112 |
| V−S | 2.364, 2.366 | 2.385, 2.377 | 2.385, 2.375 | 2.357, 2.385 | 2.375, 2.383 |
| bond angle, deg | | | | | |
| O−V−O | 112.3 | 107.6 | 108.3 | 110.6 | 107.0 |
| N−V−N | 162.3 | 165.1 | 164.2 | 162.4 | 165.4 |
| S−V−S | 74.7 | 74.4 | 74.2 | 74.6 | 74.3 |
| $\Phi^b$ | 26.8 | 31.5 | 30.9 | 27.2 | 32.1 |
| $\Theta^c$ | 152.7 | 155.5 | 154.9 | 153.2 | 155.9 |
| $\Omega^d$ | 148.0 | 150.8 | 150.2 | 148.6 | 151.1 |
| $\psi^e$ | 96.6 | 97.3 | 97.2 | 96.6 | 97.4 |
| $s/a^f$ | 1.361 | 1.374 | 1.372 | 1.361 | 1.376 |
| $s/h^g$ | 1.100 | 1.128 | 1.124 | 1.100 | 1.132 |

[a]Structure simulated through DFT methods at the level of theory B3P86/gen with a general basis set obtained using 6-311g for V, O, C, H, and N and 6-311+g(d) for S. [b]Twist angle: 60° for octahedral and 0° for trigonal prismatic geometry. [c]Angle formed by the donors in *trans* position with vanadium (mean value): 180° for octahedral and 135° for trigonal prismatic geometry. [d]Angle formed by the two external donor atoms of the ligand with vanadium (mean value): 180° for *mer* and 90° for *fac* isomers. [e]Angle formed by the two external donors of the ligand with the central one (mean value). [f]*s*/*a* = 1.414 for an octahedron and 1.309 for a trigonal prism. [g]*s*/*h* = 1.225 for an octahedron and 1.000 for trigonal prism.



DOI: 10.1021/acs.inorgchem.5b00359
*Inorg. Chem.* 2015, 54, 6203−6215

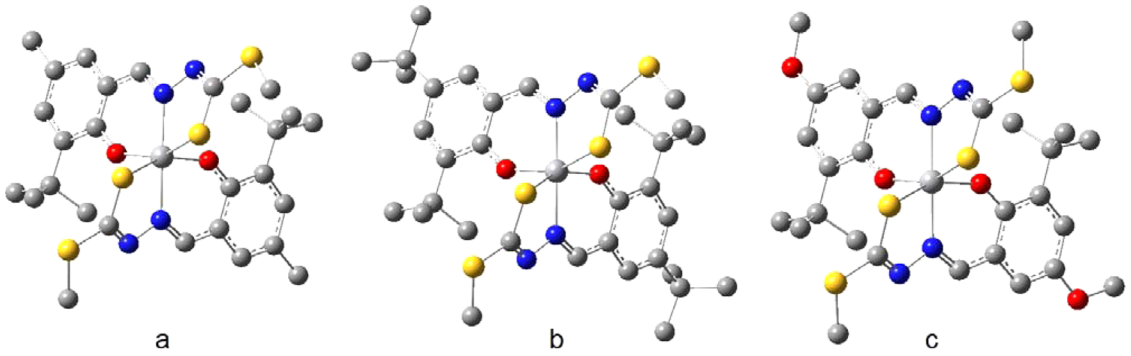


**Figure 5.** Structures of (a) **1**, (b) **2**, and (c) **3**, optimized with the DFT methods at the B3P86/gen level of theory ("gen" is a general basis set obtained using 6-311+g(d) on S and 6-311g on the other atoms). The hydrogen atoms have been omitted for clarity.

frequently for the characterization of $V^{IV}$ complexes.[30,70] The X-band EPR spectra of the complexes were recorded both at room temperature (in toluene), as well as in the frozen state (dichloroethane/toluene 1:1 v/v). A representative spectrum for compound **1** is displayed in Figure 6. Hamiltonian parameters ($g$ and $A$) determined experimentally for compounds **1**−**3** are summarized in Table 3.

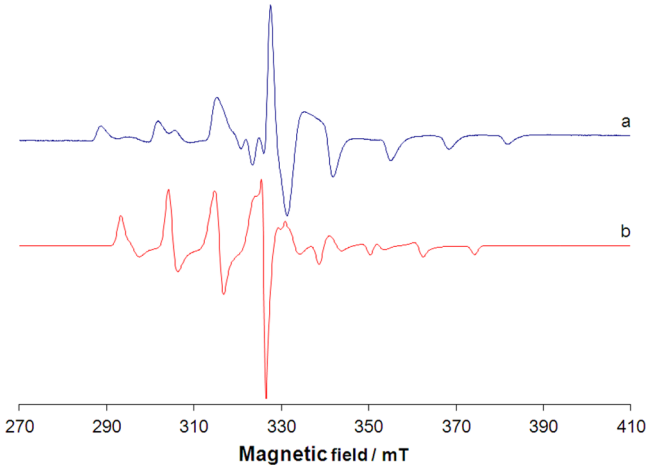


**Figure 6.** Anisotropic X-band EPR spectrum of **1**: experimental (trace a) and calculated (trace b) by DFT methods at the level of theory PBE0/VTZ. The parameters reported in Table 4 were used to generate the spectrum in trace b.

EPR spectra of hexa-coordinated $V^{IV}$ complexes can be divided into two groups: those with $g_z \ll g_x \approx g_y < 2.0023$ and $A_z \gg A_x \approx A_y$ (type 1, $d_{xy}$ ground state and geometry close to the octahedral one) and those with $g_x \approx g_y \ll g_z \approx 2.0023$ and $A_x \approx A_y \gg A_z$ (type 2, $d_{z^2}$ ground state and geometry close to the trigonal prismatic one).[71] In particular, the change in the EPR behavior has been related to the switch of the ground state from $d_{xy}$ to $d_{z^2}$, depending, in its turn, on the transformation of an octahedron toward a trigonal prism.[18d,29,72] We recently demonstrated that, for a tridentate ligand that forms nonoxido $V^{IV}$ species, *mer* isomers show type 1, whereas *fac* isomers show a type 2 spectrum.[24k] On the basis of data summarized in Table 3, **1**−**3** are characterized by an intermediate behavior with $g_x < g_y \approx g_z \ll 2.0023$ and $A_x > A_y \gg A_z$. For this reason, for the singly occupied molecular orbital (SOMO), a mixing between V-$d_{xy}$ and V-orbitals with component along the $z$ axis is expected, caused by the distortion of the octahedral geometry toward the trigonal prismatic one.

Nowadays, the prediction of $^{51}V$ hyperfine coupling constant tensor **A** is possible through the DFT methods. For a nonoxido $V^{IV}$ species, a calculation with ORCA software, which includes the second-order spin−orbit effects, using PBE0 functional and VTZ basis set gives a good agreement with the experimental data.[20b,21c,24j,k] The results are listed in Table 4.

From a comparison of Tables 3 and 4, it can be noted that DFT calculations correctly predict the order $A_x > A_y \gg A_z$. The percent deviation from the experimental value of $A_{iso}$ and $A_y$ is moderate: <4% in the first and <7% in the second one. It is slightly larger for $A_x$ (in the range of 10%−13%), but consistent with the results previously reported.[20b,21c,24j,k] In Figure 6, the comparison between the experimental (trace a) and calculated (trace b) spectrum is shown, with the difference being due to the underestimation of $A_x$ value by DFT methods (recall Table 4).

Recently, we noticed that the arrangement of the ligand molecules, *mer* or *fac*, has marked influence on the electronic structure of a nonoxido $V^{IV}$ complex.[24j,k] In particular, the values of $A$ can be correlated with the angle Ω, i.e., the angle formed at the metal center by the two external donors of the tridentate ligand, which is 180° for a *mer* isomer and 90° for a *fac* isomer. The values of $A_i$ ($i = x, z$), as a function of Ω for some tridentate ligands, are shown in Figure 7. Three types of ligands were considered: (i) cyclic ligands that form *fac* structures, such as 1,3,5-triamino-1,3,5-trideoxy-*cis*-inositol

**Table 3. Experimental $g$ Factors and $^{51}V$ Hyperfine Coupling Constants ($A$) for Complexes 1−3[a]**

| complex | $g_{iso}$ | $g_{iso}^{expct}$[b] | $g_x$ | $g_y$ | $g_z$ | $A_{iso}$ | $A_{iso}^{expct}$[c] | $A_x$ | $A_y$ | $A_z$ |
|---|---|---|---|---|---|---|---|---|---|---|
| **1** | 1.958 | 1.957 | 1.941 | 1.964 | 1.967 | −65.8 | −64.6 | −119.6 | −91.2 | 17.0 |
| **2** | 1.957 | 1.957 | 1.940 | 1.964 | 1.967 | −67.1 | −65.9 | −119.8 | −91.8 | 14.0 |
| **3** | 1.958 | 1.958 | 1.942 | 1.964 | 1.967 | −65.0 | −64.6 | −120.0 | −89.8 | 16.0 |

[a]Values of $A$ reported in terms of $10^{-4}$ $cm^{-1}$. [b]$g_{iso}^{expct}$ is the value of $g_{iso}$ expected on the basis of the formula $g_{iso} = {}^1/_3(g_x + g_y + g_z)$, with $g_x$, $g_y$, $g_z$ measured from the anisotropic spectrum. [c]$A_{iso}^{expct}$ is the value of $A_{iso}$ expected on the basis of the formula $A_{iso} = {}^1/_3(A_x + A_y + A_z)$, with $A_x$, $A_y$, $A_z$ measured from the anisotropic spectrum.



DOI: 10.1021/acs.inorgchem.5b00359
*Inorg. Chem.* 2015, 54, 6203−6215

Table 4. Calculated $g$ Factors and $^{51}$V Hyperfine Coupling Constants ($A$) with DFT Methods for Complexes 1−3[a,b]

| complex | $g_{iso}$ | $g_x$ | $g_y$ | $g_z$ | $A_{iso}$ | $A_x$ | $A_y$ | $A_z$ | $\%\lvert A_{iso}\rvert$[c] | $\%\lvert A_x\rvert$[c] | $\%\lvert A_y\rvert$[c] |
|---|---|---|---|---|---|---|---|---|---|---|---|
| 1 | 1.968 | 1.949 | 1.975 | 1.981 | −66.7 | −105.3 | −87.0 | −7.9 | +1.4 | −12.0 | −4.6 |
| 2 | 1.969 | 1.950 | 1.975 | 1.981 | −66.5 | −104.3 | −87.8 | −7.5 | −0.9 | −12.9 | −4.4 |
| 3 | 1.968 | 1.949 | 1.976 | 1.981 | −67.1 | −108.0 | −84.0 | −9.3 | +3.2 | −10.0 | −6.5 |

[a]Calculations performed at the level of theory PBE0/VTZ. [b]Values of $A$ reported in terms of $10^{-4}$ cm$^{-1}$. [c]Percent deviation from the experimental value (see Table 3) calculated as $100 \times [(\lvert A_i\rvert^{calcd} - \lvert A_i\rvert^{exptl})/\lvert A_i\rvert^{exptl}]$, with $i$ = iso, $x$, or $y$.

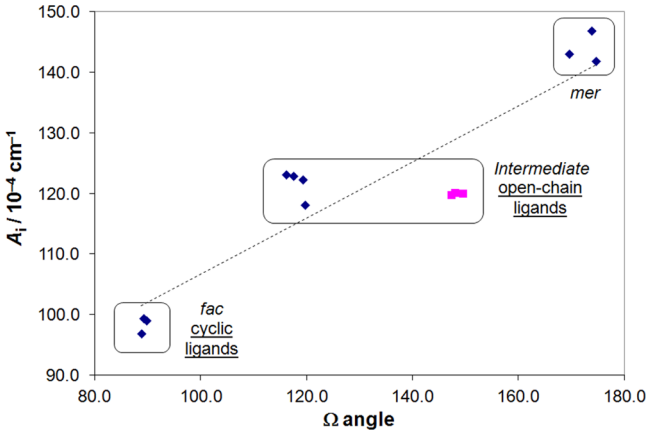


**Figure 7.** $A_i$ (as the absolute values) for nonoxido V$^{IV}$ complexes as a function of the angle Ω. The pink squares indicate complexes **1**−**3**. $A_i$ ($i$ = $x$ or $z$) is the largest values of the $^{51}$V hyperfine coupling tensor **A**. The dotted gray line represents the best linear fitting of the 13 points.

(taci),[26a] 1,3,5-trideoxy-1,3,5-tris(dimethylamino)-*cis*-inositol (tdci),[26a] and *cis*-inositol (ino);[26b] (ii) open-chain ligands that form *fac* structures, such as 2,2′-dihydroxyazobenzene (Hdhab),[24k] α-(2-hydroxy-5-methylphenylimino)-*o*-cresol (Hhmpic),[24k] calmagite ($H_2$calm),[24k] anthracene chrome red A ($H_3$anth),[24k] and complexes **1**−**3**; and (iii) open-chain ligands that form *mer* structures, such as 3,5-bis(2-hydroxyphenyl)-1-phenyl-1*H*-1,2,4-triazole ($H_2$hyph$^{Ph}$),[24j] 2,6-bis(2-hydroxyphenyl)pyri-dine ($H_2$bhpp),[24j] and bis(3,5-dimethyl-2-hydroxyphenyl)trimethylamine ($H_2L^N$).[24h] From an examination of Figure 7, a correlation between $A_i$ and Ω emerges. The ligands can be divided into three groups: on one end of the plot, the meridional complexes, characterized by Ω values of ∼180° and $A_i$ ($A_z$) larger than 140 × $10^{-4}$ cm$^{-1}$; on the other end, the facial complexes formed by cyclic ligands, characterized by Ω values of ∼90° and $A_i$ ($A_x$) smaller than 100 × $10^{-4}$ cm$^{-1}$; and, in the middle, the facial species formed by open-chain ligands, characterized by intermediate values of Ω (110°−160°) and $A_i$ ((110−130) × $10^{-4}$ cm$^{-1}$). The results in Figure 7 confirm that the EPR behavior of nonoxido V$^{IV}$ compounds is more influenced by the angle Ω than the twist angle Φ. As expected, for **1**−**3**, which are characterized by Ω values of ∼150° and a geometry intermediate between the *mer* and *fac* isomers, values of $A_x$ in the range of (110−130) × $10^{-4}$ cm$^{-1}$ are expected.

**Prediction of the Electronic Structure of Compounds 1−3.** For a distorted octahedral V$^{IV}$O complex, such as $[VO(H_2O)_5]^{2+}$, the energy order of the five $d$ orbitals is $d_{xy}$ < $d_{xz} \approx d_{yz}$ < $d_{x^2-y^2}$ < $d_{z^2}$,[73,74] the SOMO being the $d_{xy}$ orbital. For a nonoxido V$^{IV}$ species with a hexacoordinated geometry distorted toward a trigonal prismatic one, an increasing mixing of $d_{xy}$ with the excited orbitals, such as $d_{xz}$, $d_{yz}$, and $d_{z^2}$, is expected.[71]

The analysis of the electronic structure and molecular orbital composition for compounds **1**−**3** has been carried out choosing a coordinate system in which the N−V−N direction is oriented along the $z$-axis, and two S−V−O directions roughly occupy the $x$- and $y$-axes. The energy levels of the molecular orbitals (MOs) derived from V-$d$ orbitals are shown in Scheme 3. For

**Scheme 3. Relative Energy Levels of V-$d$ Orbitals for Compounds 1−3[a]**

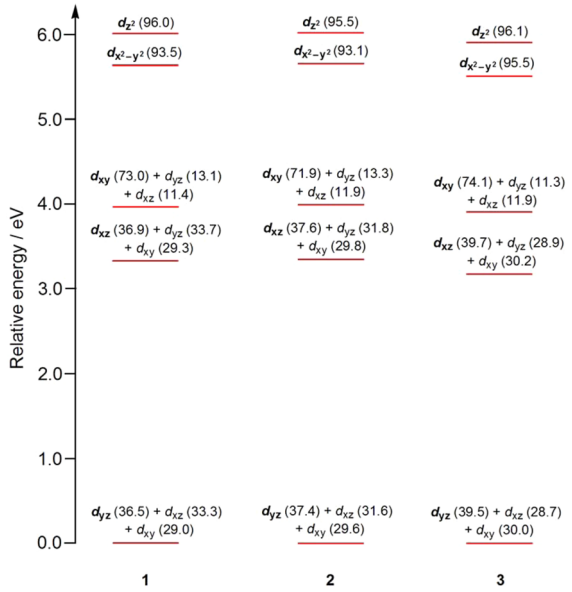


[a]Boldface font indicates the V-$d$ atomic orbital that contributes the most to the MO. Values shown in parentheses represent the total percentage contribution of the V-$d$ orbital, with respect to the total V contribution in the specific MO.

the sake of clarity, the energy of the MOs is relative to SOMO, set as reference at 0.0 eV. The percentage amount reported refers to the total contribution of V orbitals in the specific MO. For example, in the molecular orbital LUMO+5, the percentage contribution of V orbitals is 61.9% and, of this amount, 59.4% belongs to $d_{z^2}$ (relative contribution of 96.0% among V orbitals). Therefore, it can be considered that LUMO+5 is derived exclusively from V-$d_{z^2}$. Also, LUMO+4 is derived almost exclusively from V-$d_{x^2-y^2}$. In the other cases (SOMO, LUMO, and LUMO+1), the contribution of V atomic orbitals is divided between $d_{xy}$, $d_{xz}$, and $d_{yz}$ (this mixing results in a lowering of the $^{51}$V hyperfine coupling constant discussed below).

The energy order of the five MOs originated from V-$d$ orbitals is very similar, and it is $d_{yz,xz}$ < $d_{xz,yz}$ < $d_{xy}$ < $d_{x^2-y^2}$ < $d_{z^2}$. Only for compound **3**, a slight decrease of the energy of the virtual orbitals, with respect to the SOMO, set at 0.0 eV, is predicted. It can be observed that, whereas $d_{x^2-y^2}$ and $d_{z^2}$ are not combined with other $d$ orbitals, a strong mixing among $d_{xy}$, $d_{xz}$,


DOI: 10.1021/acs.inorgchem.5b00359
Inorg. Chem. 2015, 54, 6203−6215

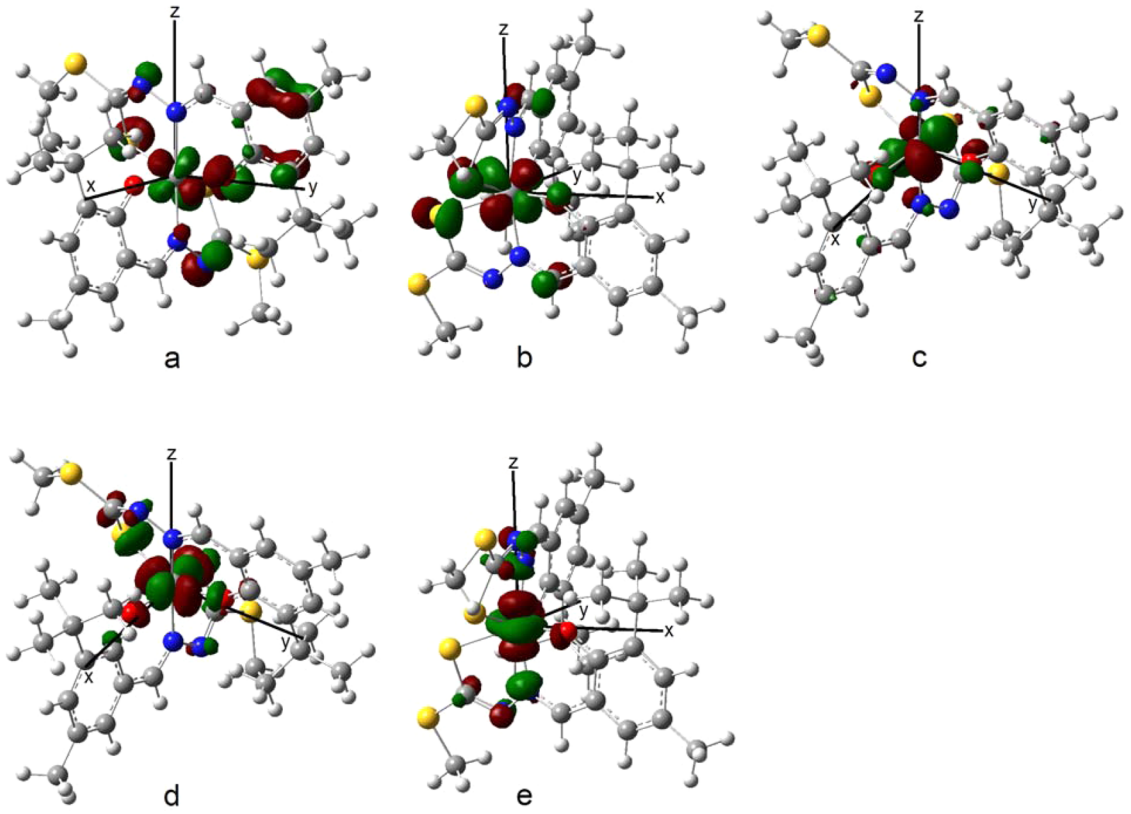


**Figure 8.** Molecular orbitals for **1**: (a) SOMO (mixing of V-$d_{xy}$, V-$d_{xz}$, and V-$d_{yz}$); (b) LUMO (mixing of V-$d_{xy}$, V-$d_{xz}$, and V-$d_{yz}$); (c) LUMO+1 (mixing of V-$d_{xy}$, V-$d_{xz}$, and V-$d_{yz}$); (d) LUMO+4 (V-$d_{x^2-y^2}$); and (e) LUMO+5 (V-$d_{z^2}$).

and $d_{yz}$ orbital exists and all the three atomic orbitals contribute with a comparable percentage to the composition of the MOs SOMO, LUMO, and LUMO+1. In particular, such a mixing is rather evident in LUMO+1 (Figure 8c), where it is observable that this MO does not occupy only *xy* but also *xz* and *yz* planes. In Figure 8, some selected molecular orbitals for **1** are shown.

From these results, it emerges that the mixing of V-$d_{xy}$, V-$d_{xz}$, and V-$d_{yz}$ orbitals in the SOMO takes place. The lowering of the $A_i$ values (here, for the sake of simplicity, $i = z$; see Figure 7) for compounds **1**−**3**, with respect to the hyperfine coupling constant of a $V^{IV}O$ complex, is due to the linear combination of V-$d_{xy}$ and V-$d_{yz}$/V-$d_{xz}$ orbitals. It can be explained considering that $A_z \propto P_d \times \beta^2(-\kappa - 2/7)$ when the SOMO is a pure V-$d_{xy}$ orbital and that $A_z \propto P_d \times \gamma^2(-\kappa + 2/7)$ when the SOMO is a pure V-$d_{yz}$ orbital, with $P_d$ being the dipolar term ($128 \times 10^{-4}$ $cm^{-1}$ for $V^{IV}$),[75] $\kappa$ being the isotropic or Fermi contact (∼0.85 for $V^{IV}$),[75] and $\beta$ and $\gamma$, the coefficients of the atomic orbital in the SOMO.[70c] It must be noticed that, in the first case, −4/7 is added to $-\kappa$ to give a negative term large in absolute value, whereas in the second one, 2/7 is added to $-\kappa$ to give a negative term but smaller than the previous one in absolute value. For example, if for $P_d$ and $\kappa$ the values reported by Pecoraro and co-workers are used,[75] $A_z \propto -\beta^2 \times 182 \times 10^{-4}$ $cm^{-1}$ when SOMO is based on V-$d_{xy}$ orbital, $A_z \propto -\beta^2 \times 72 \times 10^{-4}$ $cm^{-1}$ when SOMO is based on V-$d_{yz}$ orbital. Therefore, the mixing of V-$d_{xy}$ with V-$d_{yz}$ orbital in the SOMO causes a marked lowering of the absolute value (experimentally measured) of the $^{51}V$ hyperfine coupling constant along the *z*-axis. As an example, if SOMO is composed by 50% V-$d_{xy}$ and 50% V-$d_{yz}$, $A_z \propto -\beta^2 \times 127 \times 10^{-4}$ $cm^{-1}$, which is comparable with the experimental values for **1**−**3**.

**Prediction of the UV-vis Spectrum.** The electronic absorption spectra of complexes **1**−**3** are grossly identical. A representative spectrum for compound **1** recorded in toluene between 270 nm and 850 nm shows a broad absorption in the visible range with a main band centered at 575 nm and a shoulder at ca. 645 nm, and two other absorptions at ca. 380 (shoulder) and 308 nm in the near UV region (see Figure 9). Attempts have been made to simulate this spectrum by TD-DFT methods, according to procedures reported in the literature.[18g,21c,49e,76] The functionals and basis sets used are listed in the Experimental and Computational Section. Thus, in Figure 9, also shown are the spectra calculated with one long-range corrected functional (CAM-B3LYP), one half-and-half hybrid functional (BHandHLYP), and one hybrid functional (B1LYP) for comparison. It can be noticed that the UV band is predicted by all the functionals; in contrast, the absorptions in the visible region are well-reproduced by CAM-B3LYP, whereas BHandHLYP and B1LYP predict too low energies for them. Generally, the order of performance of the tested functionals is long-range corrected > half-and-half hybrid > hybrid > standalone.

Differently from an oxidovanadium(IV) species, for which the bands observed in the visible range (up to 400 nm) are mainly pure *d*−*d* transitions with very low oscillator strength (corresponding to a molar absorption coefficient lower than 200 $M^{-1}$ $cm^{-1}$), for **1**, the absorptions in the 400−800 nm region are mainly ligand-to-metal charge transfer (LMCT) transitions with large values of the oscillator strength ($\varepsilon$ > 2000 $M^{-1}$ $cm^{-1}$), particularly those from the molecular orbitals formed by the $\pi$-system of imine and a lone pair of S (all perpendicular to the backbone of the ligand) toward the orbitals V-$d_{xz}$, V-$d_{yz}$, and V-$d_{xy}$. This finding confirms what has


DOI: 10.1021/acs.inorgchem.5b00359
*Inorg. Chem.* 2015, 54, 6203−6215

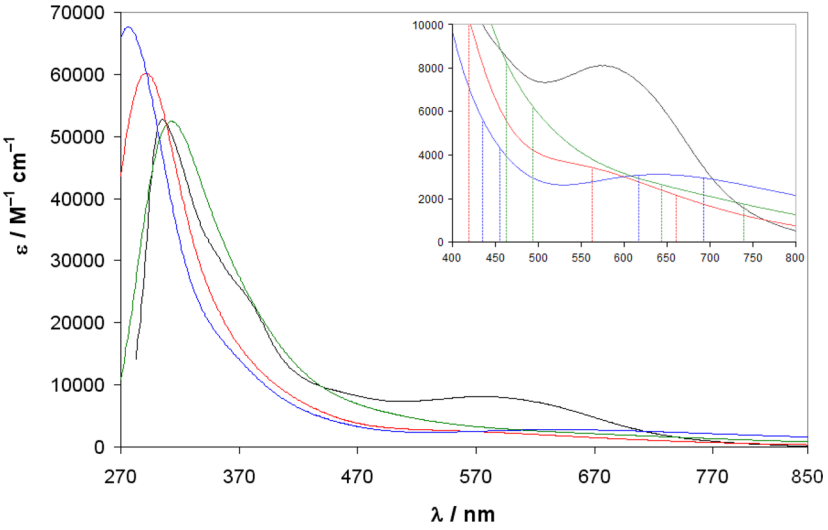


**Figure 9.** Experimental and calculated electronic absorption spectra of **1** (legend: black, the experimental spectrum; red, spectrum calculated by the CAM-B3LYP functional; blue, spectrum calculated by the BHandHLYP functional; and green, spectrum calculated by the B1LYP functional). In the inset, the visible regions (400−800 nm) of these spectra are shown in magnified scale; the transitions predicted by the three functionals are indicated by the dotted lines.

**Table 5. Main Calculated and Experimental Electronic Transitions for 1, up to 300 nm[a]**

| main transition | character[b] | $\lambda^c$ | $f$ ($\times 10^5$)[d] | $\lambda^{exptl}/\varepsilon^{exptlc,e}$ |
|---|---|---|---|---|
| H($\alpha$) → L($\alpha$)/H-1($\alpha$) → L($\alpha$) | $\pi(N_{imine})$ + lp(S) → V-$d_{xz}$/lp(S) → V-$d_{xz}$ | 666.6 | 880 | 645/6170 sh[f] |
| H-1($\alpha$) → L($\alpha$) | lp(S) → V-$d_{xz}$ | 563.1 | 1110 | 575/8100 |
| H($\beta$) → L($\beta$) | $\pi(N_{imine})$ + lp(S) → V-$d_{xz}$/lp(S) → V-$d_{xz}$ | 416.8 | 1300 | 380/23220 sh[f] |
| H-1($\beta$) → L($\beta$) | $\pi(N_{imine})$ + lp(S) + $\pi$(phenol) → V-$d_{xz}$/lp(S) → V-$d_{xz}$ | 411.2 | 3030 | |
| H-2($\beta$) → L+2($\beta$)/H-1($\beta$) → L+1($\beta$) | lp(S) → V-$d_{xy}$/$\pi(N_{imine})$ + lp(S) + $\pi$(phenol) → $\pi^*$(imine) | 343.7 | 5040 | |
| H-2($\beta$) → L+1($\beta$)/H-1($\beta$) → L+2($\beta$) | lp(S) → $\pi^*$(imine)/$\pi(N_{imine})$ + lp(S) + $\pi$(phenol) → V-$d_{xy}$ | 334.3 | 4210 | |
| H-10($\alpha$) → L+1($\alpha$) | $\pi$(phenol) → V-$d_{xy}$ | 302.1 | 9810 | 308/52320 |

[a]Calculations performed at the level of theory CAM-B3LYP/gen, with "gen" indicating a general basis set obtained using 6-31+g(d) for S and 6-31g for all the other elements. [b]"lp" indicates a lone pair; even if L($\alpha$) and L+1($\alpha$) are formed by the combination of V-$d_{xy}$, V-$d_{xz}$, V-$d_{yz}$ orbitals, we indicated, for them, only V-$d_{xz}$ and V-$d_{xy}$, which, among the three orbitals, have the largest contribution in the specific MO. [c]$\lambda$ values measured in nm. [d]Oscillator strength. [e]$\varepsilon$ measured in $M^{-1}$ $cm^{-1}$. [f]sh indicates a shoulder of a more intense absorption.

**Table 6. Summary of Electrochemical Data[a]**

| | Process A | | Process B | | | Process C | |
|---|---|---|---|---|---|---|---|
| compound | $(E_{1/2})_I$ (V)[b] | $\Delta E_p$ (mV)[c] | $(E_{1/2})_{II}$ (V)[b] | $\Delta E_p$ (mV)[c] | $n$ | $(E_{1/2})_{III}$ (V)[b] | $\Delta E_p$ (mV)[c] |
| **1** | +1.06 | 120 | −0.085 | 130 | 0.98 ± 0.03 | −1.66 | 120 |
| **2** | +1.06 | 120 | −0.086 | 110 | 0.97 ± 0.05 | −1.67 | 110 |
| **3** | +1.02 | 90 | −0.106 | 95 | 1.01 ± 0.03 | −1.66 | 100 |

[a]All potentials vs. Ag/AgCl reference. [b]$E_{1/2} = 0.5(E_{pc} + E_{pa})$, calculated from CV data. [c]$\Delta E_p = E_{pa} - E_{pc}$ at a scan rate of 200 mV $s^{-1}$.

been proposed by Raymond and co-workers, i.e., that for nonoxido vanadium(IV) species, all the transitions must be considered LMCT in which the metal orbitals involved are $d_{xy}$, $d_{xz}$, $d_{yz}$, and $d_{x^2-y^2}$ (see Table 5 and Scheme 3).[18e] The oscillator strength for the excitations in the visible range was generally more than 3 orders of magnitude larger than that for the $V^{IV}O$ complexes (for example, $\varepsilon$ is >10 000 $M^{-1}$ $cm^{-1}$ at 400 nm and >50 000 $M^{-1}$ $cm^{-1}$ at 300 nm). Even if, as observable in Figure 9, a quantitative agreement with the experiments cannot be obtained, TD-DFT calculations reproduce the experimental spectrum well, mainly if a long-range corrected functional such as CAM-B3LYP is used. In Table 5, the most important calculated electronic transitions, expressed by absorption wavelength and oscillator strength, are compared with the experimental results.

**Electrochemistry.** Cyclic voltammograms of compounds **1**−**3** have been recorded at a glassy carbon working electrode under an atmosphere of purified dinitrogen in dichloroethane solution (0.1 M TBAP) at 25 °C in the potential range from −2.0 V to +1.5 V vs. Ag/AgCl reference. The ligands are electrode active in this potential range, showing an irreversible reduction wave at a potential of $E_{pc} \approx -1.65$ V (see Figure S1 in the Supporting Information). All three compounds showed similar voltammetric features, each displaying three electrochemical responses: two in the cathodic potential range and one in the anodic potential range. The data are summarized in Table 6. The voltammogram for compound **1** is shown in Figure 10a, as a representative example, and that for compound **2** is displayed in Figure S2 in the Supporting Information. It involves an oxidation process at $(E_{1/2})_I = +1.06$ V (process A) and a couple of reduction processes at $(E_{1/2})_{II} = -0.085$ V



DOI: 10.1021/acs.inorgchem.5b00359
Inorg. Chem. 2015, 54, 6203−6215

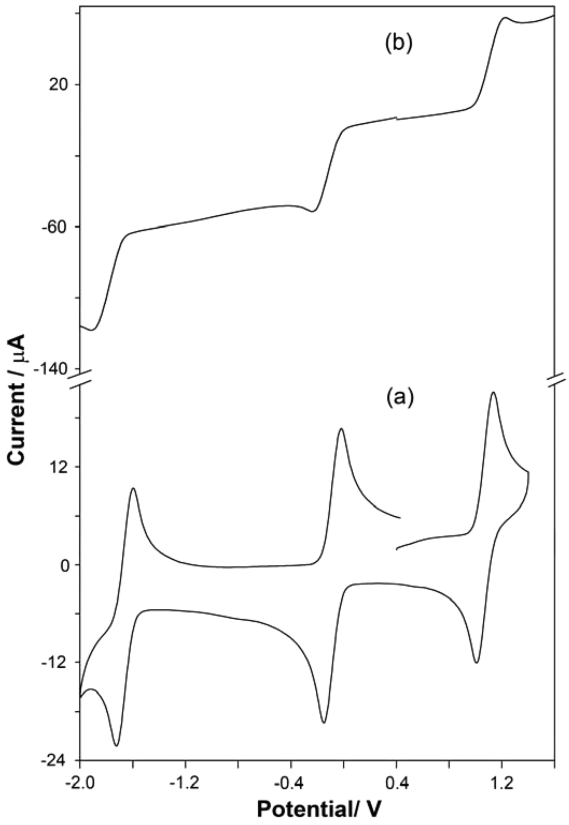


**Figure 10.** (a) Cyclic and (b) normal pulse voltammogram of compound **1** in dichloroethane. Potentials vs. Ag/AgCl, 0.1 M TBAP at a glassy carbon working electrode, scan rate: 200 mV $s^{-1}$.

(process B) and $(E_{1/2})_{III} = -1.66$ V (process C). While process A is anodic, the processes B and C appear to be cathodic, as revealed from their differential pulse voltammograms (shown in Figure 11 for compound **2** as representative example) as well as

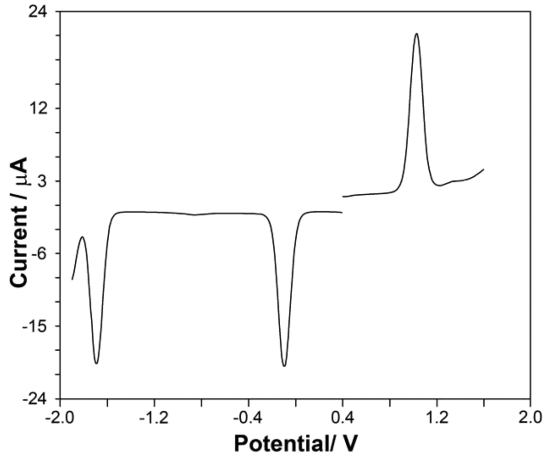


**Figure 11.** Differential pulse voltammogram of compound **2** in dichloroethane at 298 K, peak to peak amplitude is 25 mV.

from their steady-state voltammograms (using an ultramicroelectrode, 10 $\mu$M diameter), all involving an identical number of electron(s), also established by normal pulse voltammetry (NPV), shown in Figure 10b. On the basis of comparison with the ferrocenium/ferrocene couple ($\Delta E_p$ = 95 mV at a scan rate of 200 mV $s^{-1}$), all the electrochemical responses in compounds **1** and **2** may be appropriately described as quasi-reversible ($\Delta E_p$ ranges between 110 and 130 mV), while those with compound **3** are almost reversible. The reversibility of one-electron oxidation and reduction has been already observed in the literature for some other nonoxido $V^{IV}$ complexes and can be explained postulating that the "bare" vanadium structure is maintained during the redox processes.[77]

Electron stoichiometry for the reduction process B of **1**−**3** has been confirmed by constant potential coulometric (CPC) experiments with a platinum-gauze working electrode, done at a potential past the reduction process ($E_w$ set at −0.4 V vs. Ag/AgCl). Results ($n$ = 0.98 ± 0.03 for **1**, 0.97 ± 0.05 for **2** and 1.01 ± 0.03 for **3**) are in conformity with the single-electron stoichiometry for this process. Unfortunately, no meaningful results have been obtained by CPC experiments for the remaining two processes (A and C) due to unidentified electrode reaction(s). However, combining the results of differential and normal pulse voltammetry, as well as those of CPC, one can conveniently conclude that all the three electrochemical responses in these compounds have monoelectron stoichiometry, as summarized by eq 1.

$$[V^{III}L\dot{L}]^{2-} \underset{(E_{1/2})_{III}}{\overset{\text{Process C}\ +e^-}{\rightleftharpoons}} [V^{III}L_2]^{-} \underset{(E_{1/2})_{II}}{\overset{\text{Process B}\ +e^-}{\rightleftharpoons}} [V^{IV}L_2]^{0} \underset{(E_{1/2})_{I}}{\overset{\text{Process A}\ -e^-}{\rightleftharpoons}} [V^{V}L_2]^{+} \quad (1)$$

We believe that process A is due to a $V^{IV}/V^{V}$ oxidation, while process B is due to a $V^{IV}/V^{III}$ reduction, as reported earlier with nonoxido vanadium(IV) complexes.[24g] Process C, at a much negative potential, is possibly a ligand-based electron transfer, as observed with the free ligands (see Figure S1 in the Supporting Information).

From a closer look at Table 6, it appears that both $V^{IV}/V^{V}$ oxidation and $V^{IV}/V^{III}$ reduction are occurring almost at the same potentials in compounds **1** and **2**. However, with compound **3**, the oxidation becomes comparatively easier (at +1.02 V, compared to +1.06 V in **1** and **2**), while the corresponding reduction is somewhat difficult (occurring at −0.106 V with **3** compared to ca. −0.086 V with compounds **1** and **2**). This is as expected, because of the presence of an electron-donating methoxy group in the aromatic ring of the coordinated ligand ($H_2L^3$) that makes the $V^{IV}$ center in **3** comparatively electron richer.

## CONCLUSIONS

A new family of nonoxido vanadium(IV) compounds with $[V^{IV}L_2]$ stoichiometry (**1**−**3**) have been synthesized using dithiocarbazate-based tridentate biprotic Schiff-base ligands $H_2L^1$−$H_2L^3$ and structurally characterized by single-crystal X-ray diffraction analyses, which reveal a rare distorted trigonal prismatic geometry[24e,l,78] for these compounds. The spectroscopic properties (both EPR and electronic absorption spectra) of these compounds are quite unusual, compared to the $V^{IV}O$ compounds having $d_{xy}$ ground state. Their electronic spectra in the visible region feature several high-intensity (LMCT-type) bands, compared to low-intensity $d$−$d$ bands of the oxido vanadium(IV) compounds. Furthermore, the anisotropic EPR spectra are characterized by a significantly smaller value of the $^{51}V$ hyperfine coupling constant ($(119-120) \times 10^{-4}$ $cm^{-1}$) than that for $V^{IV}O$ species (usually in the range of $(150-180) \times 10^{-4}$ $cm^{-1}$). Experimental EPR spectra have been simulated by rigorous DFT calculations. The results suggest a mixing of V-$d_{xy}$, V-$d_{xz}$, and V-$d_{yz}$ orbitals in the singly occupied molecular


DOI: 10.1021/acs.inorgchem.5b00359
Inorg. Chem. 2015, 54, 6203−6215

orbital (SOMO), which causes a marked lowering of the absolute value of the $^{51}V$ hyperfine coupling constant along the *x*-axis. This peculiar electronic structure is due to the isomerism intermediate between *mer* and *fac* imposed by the open-chain $H_2L^1$−$H_2L^3$ ligands. DFT methods indicate also that a good agreement between the calculated and experimental electronic absorption spectra can be obtained if the TD-DFT calculations are carried out using a long-range corrected functional such as CAM-B3LYP. Their redox property is characterized by three electron-transfer processes, each of monoelectron stoichiometry: one in the anodic potential range due to the $V^{IV}/V^{V}$ oxidation and two in the cathodic range due to the $V^{IV}/V^{III}$ and a ligand-based reduction. The $V^{IV}/V^{V}$ oxidation and $V^{IV}/V^{III}$ reduction are quasi-reversible in nature suggesting that the "bare" structure is maintained during these redox processes.

## ■ ASSOCIATED CONTENT

### Supporting Information

Cyclic voltammogram of the free ligand ($H_2L^2$), as well as that of compound **2** (Figures S1 and S2, respectively); metrical parameters for the complexes **1** and **3** (Table S1); and X-ray crystallographic files in CIF format for compounds **1** and **3**. The Supporting Information is available free of charge on the ACS Publications website at DOI: 10.1021/acs.inorgchem.5b00359.

## ■ AUTHOR INFORMATION


### Corresponding Authors

*E-mail: garribba@uniss.it (E. Garribba).
*E-mail: icmc@iacs.res.in (M. Chaudhury).


### Notes

The authors declare no competing financial interest.

## ■ ACKNOWLEDGMENTS

This work was supported by the Council of Scientific and Industrial Research (CSIR), New Delhi, India. S.K., D.M., and K.B. also thank the CSIR for the award of research fellowships. The single-crystal X-ray diffraction data were recorded on an instrument supported by DST, New Delhi, India, as a National Facility at IACS under the IRHPA program. D.S. and E.G. thank Fondazione Banco di Sardegna for the financial support (Project Prot. U924.2014/AI.807.MGB; Prat. 2014.0443).

## ■ REFERENCES


(1) Rehder, D. *Bioinorganic Vanadium Chemistry*; John Wiley & Sons, Ltd: Chichester, U.K., 2008.

(2) (a) Vilter, H. In *Vanadium and Its Role in Life*, Sigel, H., Sigel, A., Eds.; Metallic Ions in Biological Systems, Vol. *31*; Marcel Dekker: New York, 1995; pp 325−362. (b) Pecoraro, V. L.; Slebodnick, C.; Hamstra, B. In *Vanadium Compounds*; American Chemical Society: Washington, DC, 1998; Vol. *711*, pp 157−167.

(3) (a) Robson, R. L.; Eady, R. R.; Richardson, T. H.; Miller, R. W.; Hawkins, M.; Postgate, J. R. *Nature* **1986**, *322*, 388−390. (b) Eady, R. R. *Coord. Chem. Rev.* **2003**, *237*, 23−30.

(4) (a) Ueki, T.; Michibata, H. *Coord. Chem. Rev.* **2011**, *255*, 2249−2257. (b) Fattorini, D.; Regoli, F. In *Vanadium: Biochemical and Molecular Biological Approaches*; Michibata, H., Ed.; Springer: Dordrecht, The Netherlands, 2012; pp 73−92.

(5) Crans, D. C.; Smee, J. J.; Gaidamauskas, E.; Yang, L. *Chem. Rev.* **2004**, *104*, 849−902.

(6) Costa Pessoa, J.; Tomaz, I. *Curr. Med. Chem.* **2010**, *17*, 3701−3738.

(7) Rehder, D. *Future Med. Chem.* **2012**, *4*, 1823−1837.

(8) Costa Pessoa, J.; Etcheverry, S.; Gambino, D. *Coord. Chem. Rev.* **2015**, DOI: 10.1016/j.ccr.2014.12.002.

(9) Yoshikawa, Y.; Sakurai, H.; Crans, D. C.; Micera, G.; Garribba, E. *Dalton Trans.* **2014**, *43*, 6965−6972.

(10) Levina, A.; McLeod, A. I.; Kremer, L. E.; Aitken, J. B.; Glover, C. J.; Johannessen, B.; Lay, P. A. *Metallomics* **2014**, *6*, 1880−1888.

(11) (a) Sanna, D.; Micera, G.; Garribba, E. *Inorg. Chem.* **2009**, *48*, 5747−5757. (b) Sanna, D.; Micera, G.; Garribba, E. *Inorg. Chem.* **2010**, *49*, 174−187. (c) Sanna, D.; Buglyó, P.; Micera, G.; Garribba, E. *J. Biol. Inorg. Chem.* **2010**, *15*, 825−839. (d) Sanna, D.; Micera, G.; Garribba, E. *Inorg. Chem.* **2011**, *50*, 3717−3728. (e) Sanna, D.; Bíró, L.; Buglyó, P.; Micera, G.; Garribba, E. *Metallomics* **2012**, *4*, 33−36. (f) Sanna, D.; Bíró, L.; Buglyó, P.; Micera, G.; Garribba, E. *J. Inorg. Biochem.* **2012**, *115*, 87−99. (g) Sanna, D.; Micera, G.; Garribba, E. *Inorg. Chem.* **2013**, *52*, 11975−11985. (h) Sanna, D.; Serra, M.; Micera, G.; Garribba, E. *Inorg. Chem.* **2014**, *53*, 1449−1464. (i) Sanna, D.; Serra, M.; Micera, G.; Garribba, E. *Inorg. Chim. Acta* **2014**, *420*, 75−84. (j) Koleša-Dobravc, T.; Lodyga-Chruscinska, E.; Symonowicz, M.; Sanna, D.; Meden, A.; Perdih, F.; Garribba, E. *Inorg. Chem.* **2014**, *53*, 7960−7976. (k) Sanna, D.; Fabbri, D.; Serra, M.; Buglyó, P.; Bíró, L.; Ugone, V.; Micera, G.; Garribba, E. *J. Inorg. Biochem.* **2015**, DOI: 10.1016/j.jinorgbio.2014.12.021.

(12) (a) Willsky, G. R.; Goldfine, A. B.; Kostyniak, P. J.; McNeill, J. H.; Yang, L. Q.; Khan, H. R.; Crans, D. C. *J. Inorg. Biochem.* **2001**, *85*, 33−42. (b) Liboiron, B. D.; Thompson, K. H.; Hanson, G. R.; Lam, E.; Aebischer, N.; Orvig, C. *J. Am. Chem. Soc.* **2005**, *127*, 5104−5115. (c) Liboiron, B. D. In *High Resolution EPR*; Berliner, L., Hanson, G., Eds.; Springer: New York, 2009; Vol. *28*, pp 507−549. (d) Kiss, T.; Jakusch, T.; Hollender, D.; Dörnyei, A. In *Vanadium: The Versatile Metal*; American Chemical Society: Washington, DC, 2007; Vol. *974*, pp 323−339. (e) Kiss, T.; Jakusch, T.; Hollender, D.; Dornyei, A.; Enyedy, E. A.; Pessoa, J. C.; Sakurai, H.; Sanz-Medel, A. *Coord. Chem. Rev.* **2008**, *252*, 1153−1162. (f) Correia, I.; Jakusch, T.; Cobbinna, E.; Mehtab, S.; Tomaz, I.; Nagy, N. V.; Rockenbauer, A.; Costa Pessoa, J.; Kiss, T. *Dalton Trans.* **2012**, *41*, 6477−6487. (g) Mehtab, S.; Gonçalves, G.; Roy, S.; Tomaz, A. I.; Santos-Silva, T.; Santos, M. F. A.; Romão, M. J.; Jakusch, T.; Kiss, T.; Costa Pessoa, J. *J. Inorg. Biochem.* **2013**, *121*, 187−195. (h) Goncalves, G.; Tomaz, I.; Correia, I.; Veiros, L. F.; Castro, M. M. C. A.; Avecilla, F.; Palacio, L.; Maestro, M.; Kiss, T.; Jakusch, T.; Garcia, M. H. V.; Costa Pessoa, J. *Dalton Trans.* **2013**, *42*, 11841−11861. (i) Santos, M. F. A.; Correia, I.; Oliveira, A. R.; Garribba, E.; Costa Pessoa, J.; Santos-Silva, T. *Eur. J. Inorg. Chem.* **2014**, 3293−3297.

(13) Silva, J. A. L.; Silva, J. J. R. F.; Pombeiro, A. J. L. In *Vanadium: Biochemical and Molecular Biological Approaches*; Michibata, H., Ed.; Springer: Dordrecht, The Netherlands, 2012; pp 35−49.

(14) Hu, Y.; Lee, C. C.; Ribbe, M. W. *Dalton Trans.* **2012**, *41*, 1118−1127.

(15) (a) de C. T. Carrondo, M. A. A. F.; Duarte, M. T. L. S.; Costa Pessoa, J.; Silva, J. A. L.; da Silva, J. J. R. F.; Vaz, M. C. T. A.; Vilas-Boas, L. F. *J. Chem. Soc., Chem. Commun.* **1988**, 1158−1159. (b) Berry, R. E.; Armstrong, E. M.; Beddoes, R. L.; Collison, D.; Ertok, S. N.; Helliwell, M.; Garner, C. D. *Angew. Chem., Int. Ed.* **1999**, *38*, 795−797.

(16) Einsle, O.; Tezcan, F. A.; Andrade, S. L. A.; Schmid, B.; Yoshida, M.; Howard, J. B.; Rees, D. C. *Science* **2002**, *297*, 1696−1700.

(17) Allen, F. H.; Kennard, O. *Chem. Des. Autom. News* **1993**, *8*, 31−37.

(18) (a) Cooper, S. R.; Koh, Y. B.; Raymond, K. N. *J. Am. Chem. Soc.* **1982**, *104*, 5092−5102. (b) Cass, M. E.; Gordon, N. R.; Pierpont, C. G. *Inorg. Chem.* **1986**, *25*, 3962−3967. (c) Hambley, T. W.; Hawkins, C. J.; Kabanos, T. A. *Inorg. Chem.* **1987**, *26*, 3740−3745. (d) Karpishin, T. B.; Stack, T. D. P.; Raymond, K. N. *J. Am. Chem. Soc.* **1993**, *115*, 182−192. (e) Karpishin, T. B.; Dewey, T. M.; Raymond, K. N. *J. Am. Chem. Soc.* **1993**, *115*, 1842−1851. (f) Rangel, M.; Leite, A.; João Amorim, M.; Garribba, E.; Micera, G.; Lodyga-Chruscinska, E. *Inorg. Chem.* **2006**, *45*, 8086−8097. (g) Sanna, D.; Varnágy, K.; Timári, S.; Micera, G.; Garribba, E. *Inorg. Chem.* **2011**, *50*, 10328−10341.

(19) (a) Welch, J. H.; Bereman, R. D.; Singh, P. *Inorg. Chem.* **1988**, *27*, 2862−2868. (b) Broderick, W. E.; McGhee, E. M.; Godfrey, M. R.;




DOI: 10.1021/acs.inorgchem.5b00359
*Inorg. Chem.* 2015, 54, 6203−6215

Hoffman, B. M.; Ibers, J. A. *Inorg. Chem.* **1989**, *28*, 2902−2904. (c) Kondo, M.; Minakoshi, S.; Iwata, K.; Shimizu, T.; Matsuzaka, H.; Kamigata, N.; Kitagawa, S. *Chem. Lett.* **1996**, *25*, 489−490.
(20) (a) Comba, P.; Engelhardt, L. M.; Harrowfield, J. M.; Lawrance, G. A.; Martin, L. L.; Sargeson, A. M.; White, A. H. *J. Chem. Soc., Chem. Commun.* **1985**, 174−176. (b) Lodyga-Chruscinska, E.; Szebesczyk, A.; Sanna, D.; Hegetschweiler, K.; Micera, G.; Garribba, E. *Dalton Trans.* **2013**, *42*, 13404−13416.
(21) (a) Klich, P. R.; Daniher, A. T.; Challen, P. R.; McConville, D. B.; Youngs, W. J. *Inorg. Chem.* **1996**, *35*, 347−356. (b) Kang, B.-S.; Wang, X.-J.; Su, C.-Y.; Liu, H.-Q.; Wen, T.-B.; Liu, Q.-T. *Transition Met. Chem. (Dordrecht, Neth.)* **1999**, *24*, 712−717. (c) Sanna, D.; Ugone, V.; Micera, G.; Garribba, E. *Dalton Trans.* **2012**, *41*, 7304−7318.
(22) Kabanos, T. A.; Slawin, A. M. Z.; Williams, D. J.; Woollins, J. D. *J. Chem. Soc., Chem. Commun.* **1990**, 193−194.
(23) Auerbach, U.; Vedova, B. S. P. C. D.; Wieghardt, K.; Nuber, B.; Weiss, J. *J. Chem. Soc., Chem. Commun.* **1990**, 1004−1006.
(24) (a) Diamantis, A.; Manikas, M.; Salam, M.; Snow, M.; Tiekink, E. R. T. *Aust. J. Chem.* **1988**, *41*, 453−468. (b) Kabanos, T. A.; Slawin, A. M. Z.; Williams, D. J.; Woollins, J. D. *J. Chem. Soc., Dalton Trans.* **1992**, 1423−1427. (c) Neves, A.; Ceccato, A. S.; Vencato, I.; Mascarenhas, Y. P.; Erasmus-Buhr, C. *J. Chem. Soc., Chem. Commun.* **1992**, 652−654. (d) Bruni, S.; Caneschi, A.; Cariati, F.; Delfs, C.; Dei, A.; Gatteschi, D. *J. Am. Chem. Soc.* **1994**, *116*, 1388−1394. (e) Ludwig, E.; Hefele, H.; Uhlemann, E.; Weller, F.; Kläi, W. *Z. Anorg. Allg. Chem.* **1995**, *621*, 23−28. (f) Hefele, H.; Ludwig, E.; Uhlemann, E.; Weller, F. *Z. Anorg. Allg. Chem.* **1995**, *621*, 1973−1976. (g) Farahbakhsh, M.; Schmidt, H.; Rehder, D. *Chem. Commun.* **1998**, 2009−2010. (h) Paine, T. K.; Weyhermüller, T.; Bill, E.; Bothe, E.; Chaudhuri, P. *Eur. J. Inorg. Chem.* **2003**, 4299−4307. (i) Jin, Y.; Lah, M. S. *Eur. J. Inorg. Chem.* **2005**, 4944−4952. (j) Pisano, L.; Varnagy, K.; Timári, S.; Hegetschweiler, K.; Micera, G.; Garribba, E. *Inorg. Chem.* **2013**, *52*, 5260−5272. (k) Sanna, D.; Várnagy, K.; Lihi, N.; Micera, G.; Garribba, E. *Inorg. Chem.* **2013**, *52*, 8202−8213. (l) Dash, S. P.; Pasayat, S.; Bhakat, S.; Roy, S.; Dinda, R.; Tiekink, E. R. T.; Mukhopadhyay, S.; Bhutia, S. K.; Hardikar, M. R.; Joshi, B. N.; Patil, Y. P.; Nethaji, M. *Inorg. Chem.* **2013**, *52*, 14096−14107.
(25) Paine, T. K.; Weyhermüller, T.; Slep, L. D.; Neese, F.; Bill, E.; Bothe, E.; Wieghardt, K.; Chaudhuri, P. *Inorg. Chem.* **2004**, *43*, 7324−7338.
(26) (a) Morgenstern, B.; Steinhauser, S.; Hegetschweiler, K.; Garribba, E.; Micera, G.; Sanna, D.; Nagy, L. *Inorg. Chem.* **2004**, *43*, 3116−3126. (b) Morgenstern, B.; Kutzky, B.; Neis, C.; Stucky, S.; Hegetschweiler, K.; Garribba, E.; Micera, G. *Inorg. Chem.* **2007**, *46*, 3903−3915.
(27) Westrup, K. C. M.; Gregorio, T.; Stinghen, D.; Reis, D. M.; Hitchcock, P. B.; Ribeiro, R. R.; Barison, A.; Back, D. F.; de Sa, E. L.; Nunes, G. G.; Soares, J. F. *Dalton Trans.* **2011**, *40*, 3198−3210.
(28) Kajiwara, T.; Wagner, R.; Bill, E.; Weyhermuller, T.; Chaudhuri, P. *Dalton Trans.* **2011**, *40*, 12719−12726.
(29) Raymond, K. N.; Isied, S. S.; Brown, L. D.; Fronczek, F. R.; Nibert, J. H. *J. Am. Chem. Soc.* **1976**, *98*, 1767−1774.
(30) Micera, G.; Sanna, D. In *Vanadium in the Environment, Part I: Chemistry and Biochemistry*; Nriagu, J. O., Ed.; Wiley: New York, 1998; pp 131−166.
(31) (a) Dutta, S. K.; Kumar, S. B.; Bhattacharyya, S.; Tiekink, E. R. T.; Chaudhury, M. *Inorg. Chem.* **1997**, *36*, 4954−4960. (b) Dutta, S. K.; Samanta, S.; Kumar, S. B.; Han, O. H.; Burckel, P.; Pinkerton, A. A.; Chaudhury, M. *Inorg. Chem.* **1999**, *38*, 1982−1988. (c) Dutta, S. K.; Samanta, S.; Mukhopadhyay, S.; Burckel, P.; Pinkerton, A. A.; Chaudhury, M. *Inorg. Chem.* **2002**, *41*, 2946−2952. (d) Dutta, S. K.; Samanta, S.; Ghosh, D.; Butcher, R. J.; Chaudhury, M. *Inorg. Chem.* **2002**, *41*, 5555−5560. (e) Samanta, S.; Ghosh, D.; Mukhopadhyay, S.; Endo, A.; Weakley, T. J. R.; Chaudhury, M. *Inorg. Chem.* **2003**, *42*, 1508−1517. (f) Samanta, S.; Mukhopadhyay, S.; Mandal, D.; Butcher, R. J.; Chaudhury, M. *Inorg. Chem.* **2003**, *42*, 6284−6293. (g) Bhattacharya, K.; Maity, M.; Mondal, D.; Endo, A.; Chaudhury, M. *Inorg. Chem.* **2012**, *51*, 7454−7456. (h) Bhattacharya, K.; Abtab, S. M. T.; Majee, M. C.; Endo, A.; Chaudhury, M. *Inorg. Chem.* **2014**, *53*, 8287−8297 and references therein..
(32) Perrin, D. D.; Armerago, W. L. F.; Perrin, D. R. *Purification of Laboratory Chemicals*, 2nd Edition; Pergamon Press: Oxford, U.K., 1980.
(33) Ali, M. A.; Livingstone, S. E.; Phillips, D. J. *Inorg. Chim. Acta* **1973**, *7*, 179−186.
(34) Rowe, R. A.; Jones, M. M. *Inorg. Synth.* **1957**, *5*, 113−116.
(35) Gagne, R. R.; Koval, C. A.; Lisensky, G. C. *Inorg. Chem.* **1980**, *19*, 2854−2855.
(36) Sheldrick, G. M. *SADABS, Program for Empirical Absorption Correction of Area Detector Data*; University of Göttingen: Göttingen, Germany, 1996.
(37) Sheldrick, G. M. *Acta Crystallogr., Sect. A: Found. Crystallogr.* **2008**, *64*, 112−122.
(38) Sheldrick, G. M. *SHELXL-97: Program for Crystal Structure Refinements*; University of Göttingen: Göttingen, Germany, 1996.
(39) *SAINT-plus, Software Users' Guide, Version 6.0*; Bruker Analytical X-ray Systems: Madison, WI, 1999.
(40) *DIAMOND, Visual Crystal Structure Information System, Version 3.1*; Crystal Impact: Bonn, Germany, 2004.
(41) Frisch, M. J.; Trucks, G. W.; Schlegel, H. B.; Scuseria, G. E.; Robb, M. A.; Cheeseman, J. R.; Scalmani, G.; Barone, V.; Mennucci, B.; Petersson, G. A.; Nakatsuji, H.; Caricato, M.; Li, X.; Hratchian, H. P.; Izmaylov, A. F.; Bloino, J.; Zheng, G.; Sonnenberg, J. L.; Hada, M.; Ehara, M.; Toyota, K.; Fukuda, R.; Hasegawa, J.; Ishida, M.; Nakajima, T.; Honda, Y.; Kitao, O.; Nakai, H.; Vreven, T.; Montgomery, J. A., Jr.; Peralta, J. E.; Ogliaro, F.; Bearpark, M.; Heyd, J. J.; Brothers, E.; Kudin, K. N.; Staroverov, V. N.; Keith, T.; Kobayashi, R.; Normand, J.; Raghavachari, K.; Rendell, A.; Burant, J. C.; Iyengar, S. S.; Tomasi, J.; Cossi, M.; Rega, N.; Millam, J. M.; Klene, M.; Knox, J. E.; Cross, J. B.; Bakken, V.; Adamo, C.; Jaramillo, J.; Gomperts, R.; Stratmann, R. E.; Yazyev, O.; Austin, A. J.; Cammi, R.; Pomelli, C.; Ochterski, J. W.; Martin, R. L.; Morokuma, K.; Zakrzewski, V. G.; Voth, G. A.; Salvador, P.; Dannenberg, J. J.; Dapprich, S.; Daniels, A. D.; Farkas, Ö.; Foresman, J. B.; Ortiz, J. V.; Cioslowski, J.; Fox, D. J. *Gaussian 09, Revision C.01*; Gaussian, Inc.: Wallingford, CT, 2010.
(42) Becke, A. D. *J. Chem. Phys.* **1993**, *98*, 5648−5652.
(43) Perdew, J. P. *Phys. Rev. B* **1986**, *33*, 8822−8824.
(44) Krishnan, R.; Binkley, J. S.; Seeger, R.; Pople, J. A. *J. Chem. Phys.* **1980**, *72*, 650−654.
(45) (a) Bühl, M.; Kabrede, H. *J. Chem. Theory Comput.* **2006**, *2*, 1282−1290. (b) Bühl, M.; Reimann, C.; Pantazis, D. A.; Bredow, T.; Neese, F. *J. Chem. Theory Comput.* **2008**, *4*, 1449−1459.
(46) Micera, G.; Garribba, E. *Int. J. Quantum Chem.* **2012**, *112*, 2486−2498.
(47) (a) Perdew, J. P.; Burke, K.; Ernzerhof, M. *Phys. Rev. Lett.* **1996**, *77*, 3865−3868. (b) Perdew, J. P.; Burke, K.; Ernzerhof, M. *Phys. Rev. Lett.* **1997**, *78*, 1396−1396.
(48) (a) Neese, F. *Wiley Interdiscip. Rev.: Comput. Mol. Sci.* **2012**, *2*, 73−78. (b) Neese, F. *ORCA—An Ab Initio, DFT and Semiempirical Program Package, Version 3.0*; Max-Planck-Institute for Chemical Energy Conversion: Mülheim an der Ruhr, Germany, 2013.
(49) (a) Micera, G.; Garribba, E. *Dalton Trans.* **2009**, 1914−1918. (b) Micera, G.; Pecoraro, V. L.; Garribba, E. *Inorg. Chem.* **2009**, *48*, 5790−5796. (c) Micera, G.; Garribba, E. *Eur. J. Inorg. Chem.* **2010**, 4697−4710. (d) Lodyga-Chruscinska, E.; Micera, G.; Garribba, E. *Inorg. Chem.* **2011**, *50*, 883−899. (e) Micera, G.; Garribba, E. *Eur. J. Inorg. Chem.* **2011**, 3768−3780. (f) Sanna, D.; Pecoraro, V.; Micera, G.; Garribba, E. *J. Biol. Inorg. Chem.* **2012**, *17*, 773−790. (g) Sanna, D.; Buglyó, P.; Bíró, L.; Micera, G.; Garribba, E. *Eur. J. Inorg. Chem.* **2012**, 1079−1092. (h) Sanna, D.; Buglyó, P.; Tomaz, A. I.; Pessoa, J. C.; Borovic, S.; Micera, G.; Garribba, E. *Dalton Trans.* **2012**, *41*, 12824−12838. (i) Justino, G.; Garribba, E.; Costa Pessoa, J. *J. Biol. Inorg. Chem.* **2013**, *18*, 803−813.
(50) Gorelsky, S.; Micera, G.; Garribba, E. *Chem.−Eur. J.* **2010**, *16*, 8167−8180.
(51) Micera, G.; Garribba, E. *J. Comput. Chem.* **2011**, *32*, 2822−2835.


DOI: 10.1021/acs.inorgchem.5b00359
*Inorg. Chem.* 2015, 54, 6203−6215

(52) (a) Runge, E.; Gross, E. K. U. *Phys. Rev. Lett.* **1984**, *52*, 997−1000. (b) Casida, M. K. In *Recent Advances in Density Functional Methods*; Chong, D. P., Ed.; World Scientific: Singapore, 1995; Vol. *1*, pp 155−192.
(53) Van Voorhis, T.; Scuseria, G. E. *J. Chem. Phys.* **1998**, *109*, 400−410.
(54) (a) Hamprecht, F. A.; Cohen, A. J.; Tozer, D. J.; Handy, N. C. *J. Chem. Phys.* **1998**, *109*, 6264−6271. (b) Boese, A. D.; Doltsinis, N. L.; Handy, N. C.; Sprik, M. *J. Chem. Phys.* **2000**, *112*, 1670−1678. (c) Boese, A. D.; Handy, N. C. *J. Chem. Phys.* **2001**, *114*, 5497−5503.
(55) Becke, A. D. *Phys. Rev. A* **1988**, *38*, 3098−3100.
(56) Becke, A. D. *J. Chem. Phys.* **1996**, *104*, 1040−1046.
(57) Adamo, C.; Barone, V. *Chem. Phys. Lett.* **1997**, *274*, 242−250.
(58) Lee, C.; Yang, W.; Parr, R. G. *Phys. Rev. B* **1988**, *37*, 785−789.
(59) Adamo, C.; Barone, V. *J. Chem. Phys.* **1998**, *108*, 664−675.
(60) (a) Heyd, J.; Scuseria, G. E.; Ernzerhof, M. *J. Chem. Phys.* **2003**, *118*, 8207−8215. (b) Heyd, J.; Scuseria, G. E. *J. Chem. Phys.* **2004**, *121*, 1187−1192. (c) Heyd, J.; Scuseria, G. E. *J. Chem. Phys.* **2004**, *120*, 7274−7280. (d) Heyd, J.; Scuseria, G. E.; Ernzerhof, M. *J. Chem. Phys.* **2006**, *124*, 219906.
(61) Austin, A.; Petersson, G. A.; Frisch, M. J.; Dobek, F. J.; Scalmani, G.; Throssell, K. *J. Chem. Theory Comput.* **2012**, *8*, 4989−5007.
(62) Chai, J.-D.; Head-Gordon, M. *Phys. Chem. Chem. Phys.* **2008**, *10*, 6615−6620.
(63) Yanai, T.; Tew, D. P.; Handy, N. C. *Chem. Phys. Lett.* **2004**, *393*, 51−57.
(64) Dennington, R.; Keith, T.; Millam, J. M. *GaussView, Version 4.1.2*; Semichem, Inc.: Shawnee Mission, KS, 2007.
(65) (a) Selbin, J. *Chem. Rev.* **1965**, *65*, 153−175. (b) Selbin, J. *Coord. Chem. Rev.* **1966**, *1*, 293−314.
(66) (a) Steinhauser, S.; Heinz, U.; Bartholomä, M.; Weyhermüller, T.; Nick, H.; Hegetschweiler, K. *Eur. J. Inorg. Chem.* **2004**, 4177−4192. (b) Steinhauser, S.; Heinz, U.; Bartholomä, M.; Weyhermüller, T.; Nick, H.; Hegetschweiler, K. *Eur. J. Inorg. Chem.* **2005**, 2262−2262.
(67) Steinhauser, S.; Heinz, U.; Sander, J.; Hegetschweiler, K. *Z. Anorg. Allg. Chem.* **2004**, *630*, 1829−1838.
(68) Castiñeiras Campos, A.; Silica Zafra, A. G.; González Pérez, J. M.; Niclós Gutiérrez, J.; Chinea, E.; Mederos, A. *Inorg. Chim. Acta* **1996**, *241*, 39−45.
(69) Weyhermüller, T.; Paine, T. K.; Bothe, E.; Bill, E.; Chaudhuri, P. *Inorg. Chim. Acta* **2002**, *337*, 344−356.
(70) (a) Chasteen, D. N. In *Biological Magnetic Resonance*, Berliner, L. J. J.; Reuben, J., Eds.; Plenum Press: New York, 1981; Vol. *3*, pp 53−119. (b) Smith, T. S., II; LoBrutto, R.; Pecoraro, V. L. *Coord. Chem. Rev.* **2002**, *228*, 1−18. (c) Mabbs, F. E.; Collison, D. *Electron Paramagnetic Resonance of d Transition Metal Compounds*; Elsevier Science Publishers B.V.: Amsterdam, 1992.
(71) Desideri, A.; Raynor, J. B.; Diamantis, A. A. *J. Chem. Soc., Dalton Trans.* **1978**, 423−426.
(72) Companion, A. L.; Komarynsky, M. A. *J. Chem. Educ.* **1964**, *41*, 257−262.
(73) Ballhausen, C. J.; Gray, H. B. *Inorg. Chem.* **1962**, *1*, 111−122.
(74) Garribba, E.; Micera, G.; Sanna, D. *Inorg. Chim. Acta* **2006**, *359*, 4470−4476.
(75) Smith, T. S.; Root, C. A.; Kampf, J. W.; Rasmussen, P. G.; Pecoraro, V. L. *J. Am. Chem. Soc.* **2000**, *122*, 767−775.
(76) Lodyga-Chruscinska, E.; Sanna, D.; Garribba, E.; Micera, G. *Dalton Trans.* **2008**, 4903−4916.
(77) Friedrich, A.; Hefele, H.; Mickler, W.; Mönner, A.; Uhlemann, E.; Scholz, F. *Electroanalysis* **1998**, *10*, 244−248.
(78) Diamantis, A. A.; Snow, M. R.; Vanzo, J. A. *J. Chem. Soc., Chem. Commun.* **1976**, 264−265.



DOI: 10.1021/acs.inorgchem.5b00359
*Inorg. Chem.* 2015, 54, 6203−6215